haematologica
Journal of the Ferrata Storti Foundation

MYC overexpression in natural killer cell lymphoma: prognostic and therapeutic implications

by Chengfeng Bi, Yuhua Huang, Roshia Ali, Fang Wang, Xia Yang, Alyssa Bouska, Lu Xu, Xinbao Hao, Matthew A. Lunning, Wing C. Chan, Javeed Iqbal, Dennis D. Weisenburger, Julie M. Vose, and Kai Fu

Received: August 7, 2023.
Accepted: March 18, 2024.

Citation: Chengfeng Bi, Yuhua Huang, Roshia Ali, Fang Wang, Xia Yang, Alyssa Bouska, Lu Xu, Xinbao Hao, Matthew A. Lunning, Wing C. Chan, Javeed Iqbal, Dennis D. Weisenburger, Julie M. Vose, and Kai Fu. MYC overexpression in natural killer cell lymphoma: prognostic and therapeutic implications. Haematologica. 2024 Mar 28. doi: 10.3324/haematol.2023.283811 [Epub ahead of print]

MYC overexpression in natural killer cell lymphoma: prognostic and therapeutic implications

Chengfeng Bi[1*], Yuhua Huang[2,3*], Roshia Ali[1], Fang Wang[2,4], Xia Yang[2,3], Alyssa Bouska[5], Lu Xu[6,7], Xinbao Hao[8], Matthew A. Lunning[1], Wing C. Chan[9], Javeed Iqbal[5], Dennis D. Weisenburger[5] , Julie M. Vose[1], and Kai Fu[5,6]

[1]Division of Oncology & Hematology, Department of Internal Medicine, University of Nebraska Medical Center, Omaha, NE, USA

[2]State Key Laboratory of Oncology in South China, Collaborative Innovation Center for Cancer Medicine, Guangzhou, Guangdong, China

[3]Department of Pathology, Sun Yat-sen University Cancer Center, Guangzhou, Guangdong, China

[4]Department of Molecular Diagnosis, Sun Yat-sen University Cancer Center, Guangzhou, Guangdong, China

[5]Department of Pathology and Microbiology, University of Nebraska Medical Center, Omaha, NE, USA

[6]Department of Pathology, Roswell Park Comprehensive Cancer Center, Buffalo, NY, USA

[7]Department of Hematology, The First Affiliated Hospital of Hainan Medical University, Haikou, Hainan, China

[8]State Key Laboratory of Membrane Biology, School of Medicine, Tsinghua University, Beijing, China

[9]Department of Pathology, City of Hope National Medical Center, Duarte, CA, USA

Equal contribution

Chengfeng Bi and Yuhua Huang contributed equally to this work.

Corresponding authors

Chengfeng Bi, Division of Oncology & Hematology, Department of Internal Medicine, University of Nebraska Medical Center, Nebraska Medicine Fred & Pamela Buffett Cancer Center, 505 S 45th St, Omaha, NE 68105; Email: andy.bi@unmc.edu; Kai Fu, Department of Pathology, Roswell Park Comprehensive Cancer Center, 665 Elm Street, Buffalo, NY 14203; email: Kai.Fu@roswellpark.org.

Disclosure

The authors have no conflict of interest to disclose.

Contributions

CB and KF designed the experiments; CB, YH and RA performed the experiments and data analysis; FW, XY and LX assisted in performing experiments; AB assisted in data analysis; CB wrote the manuscript; XH, ML, WCC, JI, DDW and JMV advised the project and manuscript writing.

Acknowledgments

The authors acknowledge the contributions to this study of the patients and their families.

Data-sharing statement

Data on individual patients will not be shared. Other original data and protocols are available to other investigators upon request.

Funding

This study was supported by the University of Nebraska Foundation.

Abstract

The current clinical management of Extranodal NK/T-cell lymphoma (ENKTL) primarily depends on conventional chemotherapy and radiotherapy, underscoring the need for innovative therapeutic strategies. This study explores the clinical significance and therapeutic implication of c-MYC (MYC) in ENKTL. Initially, we identified MYC protein overexpression in approximately 75% of cases within a large cohort of 111 patients. MYC overexpression was strongly correlated with lymphoma cell proliferation and poor clinical outcomes. Intriguingly, integrating MYC expression into the PINK-E prognostic model significantly enhanced its predictive power. Subsequently, we implemented MYC knockdown (KD) in NK malignancy cell lines with MYC overexpression, resulting in significant viability reduction. RNA-sequencing (RNA-seq) used to determine MYC function revealed a high overlap with canonical MYC-regulated genes and enrichment in metabolism and cell cycle regulation. Integrative analysis of the RNA-seq data upon MYC KD with gene expression profiles of primary ENKTL cases identified a subset of genes closely associated with MYC overexpression. Among these, CDK4 emerged as a potential therapeutic target, and its inhibition not only abrogated MYC function but also decreased MYC expression in NK malignancy cells. Furthermore, the clinical-grade CDK4/6 inhibitor palbociclib exhibited a potent anti-tumor effect in xenograft mouse models, especially when combined with gemcitabine. In summary, our study firmly establishes MYC as an oncogene with prognostic significance in ENKTL and highlights CDK4 inhibition as a promising therapeutic strategy for treating ENKTL with MYC overexpression.

Introduction

Extranodal NK/T-cell lymphoma (ENKTL) is a distinct form of non-Hodgkin lymphoma (NHL) associated with Epstein–Barr virus (EBV) infection. The clinical outcome of patients with ENKTL is largely dependent on the clinical stage, and the median survival was only 7-20 months for those with advanced-stage disease.[1-3] Although significant advances have been made in our understanding of the pathogenesis and driver oncogenes of this disease,[4-10] treatment strategies have not led to a substantial improvement in survival. Clinical management, to a large extent, still relies on conventional chemotherapy and radiotherapy, and there is an unmet need to identify novel therapeutic approaches.

MYC is a transcription factor that promotes oncogenesis by activating and repressing downstream target genes controlling cell growth, metabolism, and survival.[11] In hematological malignancies, MYC is recognized as the essential driver in Burkitt lymphoma (BL) and high-grade B-cell lymphoma, whereas its prognostic significance in ENKTL has not been well addressed. Despite only rare genetic alterations in ENKTL, MYC may still play an important role in tumor development because of its interactions with other disease drivers. Specifically, alterations in transcription factors, including activating mutations of *STAT3* and *STAT5*, and inactivating mutations/deletion of *PRDM1* and *TP53* were found to be important driving mechanisms in the oncogenesis of ENKTL.[4, 7, 9, 10, 12] These drivers have been shown to directly regulate MYC expression, which is of considerable significance in cancer development.[10, 13-17] In particular, our recent study demonstrated that MYC expression was remarkably increased upon *PRDM1* deletion in primary NK cells.[10] Notably, a recent genomic study identified a genetic subtype of ENKTL named MB based on *MGA* mutation and 1p22.1/*BRDT* loss of heterozygosity.[9] This subtype is characterized by MYC overexpression and is associated with a poor clinical outcome. Based on these findings, we hypothesize that MYC is inclined to be transcriptionally activated by oncogenic drivers of ENKTL and that enhanced MYC expression significantly contributes to tumor biology and clinical outcome. In fact, previous studies have reported a correlation between MYC overexpression and an inferior clinical outcome in ENKTL.[18, 19] Nevertheless, the biological significance and implications in clinical practice warrant further exploration.

In this study, we enrolled a substantial ENKTL patient cohort, scrutinizing MYC expression to comprehend its implications on clinical prognosis and risk assessment. Concurrently, we profiled MYC target genes, aiming to elucidate MYC function and pinpoint potential therapeutic targets pertinent to ENKTL cases with MYC overexpression.

Methods

Patients, samples, and clinicopathological data

A cohort of 111 patients with ENKTL diagnosed between 2009 and 2019 at Sun Yat-sen University Cancer Center was retrospectively investigated. All tissue specimens were formalin-fixed and paraffin-embedded (FFPE). The histology and immunophenotype were retrieved and reviewed by two experienced hematopathologists using the WHO Classification.[20] Inclusion criteria required that cases have: 1) relevant clinical and follow-up data; 2) sufficient pathology materials for review and further analysis; and 3) no history of immunodeficiency. All patients provided written informed consent for the tissue specimen collection and publication of their medical information during the first visit to the hospital. The registry was approved by the Institutional Review Board (SL-B2022-581-01)

Gene knockdown (KD) and RNA sequencing (RNA-Seq)

For MYC and RB (RB transcriptional corepressor 1) KD, Dicer-Substrate Short Interfering RNAs (DsiRNAs) or negative control (NC1) (IDT, Coralville, IA, USA) were transfected into NK malignancy cell lines by electroporation using the Amaxa 4d nucleofector (Program CM-150). The siRNA sequences are listed in Supplementary Table S1. For RNA sequencing, total RNA was isolated and purified 48h after siRNA transfection using the RNeasy Mini Kit (Qiagen, Germantown, MD, USA). Before library preparation, RNA integrity number (RIN) was assessed using the Agilent Bioanalyzer 2100, and only RNA samples with RIN >7 were used for subsequent library preparation. Pooled libraries were sequenced by the Illumina NextSeq 500 system with PE150 reads.

In vivo experiment

All mouse experiments were approved by the Institutional Animal Care and Use Committee at the University of Nebraska Medical Center. To establish cell line-derived xenograft (CDX) and patient-derived xenograft (PDX) tumors, approximately $2x10^6$ tumor cells were subcutaneously implanted in 10-week-old NSG mice (The Jackson Laboratory, Bar Harbor, ME, USA). The PDX model was obtained from the Public Repository of Xenografts (ProXe, #DFTL-85005) with the 5th passage being used for the treatment assay. For IMC-1 CDX and PDX models, treatment was initiated 21 days post-xenograft implantation. Palbociclib was given by gavage of saline-dissolved isethionate daily, and gemcitabine was administered by *I.P.* injection of saline-dissolved hydrochloride weekly. Treatments of either drugs or saline control were continuously administered for 21 days, and the survival was monitored with the endpoints including death, body weight loss >20%, and severe morbidity. For the YT CDX model, treatments were initiated when the tumor volume reached approximately ~$100mm^3$ and were continuously administered for 14 days. Immunohistological examination was performed after treatment or at the endpoints of the experiment, with the primary antibody information detailed in Supplementary Table S2.

Additional information can be found in the Online Supplemental Appendix.

Results

MYC overexpression in ENKTL is associated with elevated cell proliferation

We retrospectively analyzed a cohort of 111 ENKTL cases, finding that most clinical characteristics aligned with prior reports[21-23] despite a slightly higher percentage of regional lymph node involvement (Table 1). MYC expression in the diagnostic samples was examined using immunohistochemistry (IHC), which showed a wide variation in the percentage of MYC-positive cells among these cases. Receiver operating characteristic (ROC) curve analysis identified 20% as the optimal cut-off value for predicting clinical outcomes, leading to the classification of 83 cases (74.9%) as exhibiting high MYC expression (Figure 1A, B). However, there was no discernible correlation between MYC expression and key clinical features (Supplementary Table S3). We also probed *MYC* rearrangement and copy number variation by FISH in 60 cases. This revealed *MYC* gene locus gain in 3 cases (5%), but no evidence of MYC gene rearrangement or amplification (Supplementary Figure S1). Considering that elevated MYC typically correlates with a higher proliferative rate, we evaluated the Ki-67 index in these cases. Defining a value of $\geq$60% as a high expression, based on the median value of this cohort, the Ki-67 index was found to be high in 63 of the 83 MYC-high cases (75.9%), compared to only one out of 28 MYC-low cases (3.6%, Figure 1A, B). A strong correlation was demonstrated between the two markers (R=0.7989, Figure 1C), suggesting that MYC overexpression is closely related to cell proliferation in ENKTL. Moreover, in the analysis of 18 cases with both diagnostic and relapse biopsy samples, we found that 13 cases (72.2%) displayed a higher percentage of MYC expression in the relapse sample (Figure 1D, E). Taken together, this data indicates that MYC protein is frequently overexpressed in ENKTL, which is associated with increased proliferation of the lymphoma cells.

MYC overexpression is a marker of inferior clinical outcome in ENKTL

The median progression-free survival (PFS) and overall survival (OS) for this cohort of patients were 28.1 and 45.4 months respectively. Notably, patients with high MYC expression exhibited significantly worse outcomes for both PFS and OS compared to those with low MYC expression (Figure 2A, B). In the subgroup analysis of patients treated with pegaspargase/asparaginase-based regimens, high MYC expression also correlated with inferior outcomes (Supplementary Figure S2). However, multivariate analysis did not identify MYC overexpression as a significant prognostic factor for either OS or PFS, suggesting potential overlap with other characteristics in this disease (Supplementary Table S4 and S5). To further explore the significance of MYC expression in clinical risk stratification, we assessed the commonly used PINK-E

model[22] in this cohort of cases and found that in general, this model was able to stratify cases with different clinical outcomes. However, a notable limitation emerged as it classified more than 76% of cases into the low-risk group, where the 3-year PFS and OS were observed to be 59.0% and 71.0%, respectively (Figure 2C, D). Interestingly, when adding MYC expression to this model, we obtained a new stratification by using the score of 0-1 for low-risk, 2-3 for intermediate-risk, and ≥ 4 for high-risk, which exhibited improved efficacy, especially for distinguishing the low-risk group (Figure 2E, F). Similarly, we examined the integration of Ki-67 and also obtained an improved stratification than PINK-E (Figure 2G, H) when using the score of 0-1 for low-risk, 2 for intermediate-risk, and ≥3 for high-risk. We designated these two indexes as PINK-EM and PINK-EK, respectively, which have the potential to serve as useful tools in the clinical management of ENKTL.

MYC overexpression mediates proliferation and survival in NK malignancy cells

To deepen our understanding of MYC overexpression in ENTKL, we conducted *in vitro* functional analyses using a spectrum of NK malignancy cell lines, encompassing both NK lymphoma and leukemia, given the substantial overlaps in morphological and genetic characteristics between these two entities, alongside normal NK cells. We observed that normal NK cells consistently showed low MYC mRNA and protein levels, in contrast to the notable variation seen in NK malignancy cells. Specifically, YT and NK-YS cells had MYC expression comparable to normal cells, while KHYG-1, NK-92, and IMC-1 cells exhibited significantly higher levels (Figure 3A, B). In pursuit of unraveling the functional role of MYC, we selected the cell lines with pronounced overexpression for MYC depletion. Given the oncogenic nature of MYC and the inherent challenges of transfecting blood cancer cells, we opted for the siRNA approach and used a blend of two siRNAs to mitigate potential off-target effects. We evaluated three siRNA mixtures in NK-92 and IMC-1 cells, which displayed the highest MYC expression levels. The three mixtures exhibited varying KD efficacy with the first one (S1) being the highest and thus being chosen for subsequent experiments (Figure 3C). Notably, all tested siRNA mixtures significantly reduced cell viability, with the extent of this reduction closely mirroring the level of MYC depletion (Figure 3C, D). Specifically, after 72 hours of transfection with the S1 mixture, cell viability in treated cells decreased to approximately one-third of that in control cells. In addition, we noted a significant increase in cell apoptosis post MYC KD, by approximately 22% and 34% in NK-92 and IMC-1 cells, respectively (Figure 3E). This indicates that MYC overexpression contributes to both the proliferation and survival of NK malignancy cells. Moreover, MYC depletion in cell lines with low to intermediate MYC expression also led to reduced cell viability, albeit less pronounced compared to cells with high MYC expression (Supplementary Figure S3), which aligns with the established role of MYC as an oncogene.

Next, we performed RNA sequencing in NK-92 and IMC-1 cells following MYC KD, revealing substantial gene expression changes in both cell lines. Specifically, 24 hours

after KD, we identified 3995 significantly altered genes in NK-92 cells, with 2474 showing decreased expression and 1521 showing an increase. In IMC-1 cells, we observed significant alterations in 4856 genes, including a decrease in expression for 2931 genes and an increase for 1925 genes (Supplementary Figure 4A). Gene Set Enrichment Analysis (GSEA) showed that the differentially expressed genes (DEGs) were highly enriched in canonical MYC target genes in both cell lines (Supplementary Figure 4B), suggesting that MYC exerts similar oncogenic functions in ENKTL as it does in other types of cancers. Comparative examination identified 1746 downregulated and 742 upregulated genes commonly shared between the two cell lines. Pathway analysis showed that the downregulated genes were primarily involved in metabolic processes and cell cycle regulation, reinforcing the pro-proliferative function of MYC (Supplementary Figure 4C). Conversely, upregulated genes were highly enriched in TNF-NF-kB and JAK-STAT signaling pathways, including both pathway activators/effectors and inhibitors, likely reflecting a feedback mechanism of oncogenic signaling (Supplementary Figure 4D). In addition, we also profiled the DEGs 48 hours after MYC KD and obtained a similar result for functional characterization (Supplementary Figure S5).

Identification of CDK4 as a potential therapeutic target in ENTKL with MYC overexpression

To confirm the identified MYC target genes, we analyzed gene expression profiling (GEP) data from 44 previously studied ENKTL cases.[5] We divided cases into three equal-sized groups according to MYC expression levels and then examined the DEGs between the 15-case subsets of low and high MYC expression groups. On average, the high-MYC group exhibited approximately six times the MYC level of the low-MYC group, with DEG analysis revealing 176 upregulated and 58 downregulated genes in the MYC-high group (Figure 4A, B). Then, we compared the DEGs between the primary cases and the cell line data, and identified a list of 68 commonly shared genes, including 66 downregulated and 2 upregulated (Figure 4C, D, Supplementary Table S6). These genes likely represent bona fide target genes associated with MYC overexpression in ENKTL and have the potential to serve as therapeutic targets to impair MYC function given that direct MYC inhibition is impractical in current clinical practice. Theoretically, an ideal target needs to meet two essential criteria: It should be intimately relevant to MYC function and be pharmacologically targetable. By a holistic evaluation of the MYC functions demonstrated in the cell experiments, we set our sights on two well-defined MYC targets, HK2 and CDK4.[24, 25] Notably, upon MYC KD, we observed a marked reduction in protein levels for both genes in the MYC-high NK lines (Figure 4E). For comparison, we also analyzed MYC-low NK lines and BL cell lines Raji and Namalwa, which harbor MYC/IgH rearrangements, revealing a reduction trend closely linked to the extent of MYC depletion (Supplementary Figure S6A). In terms of pharmacological intervention, benserazide, a drug to treat Parkinson's disease, was shown to be a selective HK2 inhibitor,[26] whereas several inhibitors targeting CDK4, such as palbociclib,

have been approved for the treatment of breast cancer. Therefore, both targets were subjected to further inhibition testing.

We treated the seven NK malignancy cell lines with escalating doses of benserazide and palbociclib and observed a cell sensitivity profile strongly correlated with MYC expression level. Specifically, cells with MYC overexpression were more susceptible to the inhibition (Figure 5A; Supplementary Figure S6B). However, the effective inhibition of benserazide required doses (>10 μM) that would be prohibitive for potential *in vivo* application. In contrast, palbociclib demonstrated superior potency with effective doses in the nanomolar range and displayed better differentiation between MYC-high and MYC-low cells. Therefore, it was subjected to further investigation, which showed that the treatment induced both cytostatic and cytotoxic effects (Figure 5B). Because CDK4 promotes cell cycle progression through phosphorylating the tumor suppressor protein Rb, thereby releasing E2F transcription factors, we examined this signaling pathway with palbociclib treatment and observed time-dependent de-phosphorylation of Rb at multiple sites (Figure 5C). Interestingly, we found that the MYC expression level was significantly decreased on both protein and mRNA levels, especially after 48 hours of treatment (Figure 5C and Supplementary Figure S6C), suggesting that MYC repression likely resulted from transcription reprogramming due to Rb activation. This is supported by the significant rescue of MYC depletion following Rb KD (Figure 5D). Moreover, we applied palbociclib treatment in Raji and Namalwa cells and found that the MYC level was barely affected (Supplementary Figure S6D). In addition, to determine whether MYC repression was a simple consequence of cell cycle arrest, we performed a double thymidine block assay but did not observe the depletion of MYC as in the palbociclib treatment (Supplementary Figure S6E). Collectively, our data indicate that active cell cycle progression mediated by the E2F transcription program is essential for MYC overexpression in NK malignancy cells, whereby a regulatory feedback loop between MYC and CDK4 is thus formed (Figure 5E).

Palbociclib suppressed tumor growth in xenograft mouse models

For *in vivo* testing, we first established the IMC-1 CDX model, in which the tumor cells mainly resided in the viscera, especially the liver (Supplementary Figure S7). Compared to the vehicle control, palbociclib treatment at 50 mg/kg significantly prolonged the survival of animals, with a 50% increase in median survival (60 days in the treatment group vs. 40 days in the control group) (Figure 6A). To assess the effectiveness under low MYC expression conditions, we conducted the treatment in the xenograft model of YT cells, characterized by minimal MYC expression. Consistent with *in vitro* data, the YT cell xenograft, which readily forms subcutaneous tumors, showed no response to the treatment (Supplementary Figure S8). To further evaluate this therapeutic effect, we employed a PDX model of ENKTL with MYC overexpression. Because in the IMC-1 CDX experiment we observed that male mice generally had longer survival, likely due to higher body weight in males at the comparable age, we performed the PDX studies separately for female and male mice. The growth pattern of

the PDX model was similar to that of the IMC-1 CDX model, with the viscera organs, especially the liver predominantly involved. Beyond palbociclib single treatment, we also explored the potential enhancement of therapeutic efficacy with a combination of palbociclib and gemcitabine, a key chemotherapeutic agent in ENKTL treatment, particularly since palbociclib primarily induces a cytostatic effect. By preliminary testing, we established a well-tolerated treatment schedule in which gemcitabine was administered as 100mg/kg on day 1, followed by palbociclib 100 mg/kg on days 4-6, continuously for 3 weeks. We found that either palbociclib or gemcitabine monotherapy, moderately prolonged the mouse survival, (median survival increases: 31%-50% in female mice and 21%-44% in male mice), whereas the combined treatment substantially improved the outcomes (median survival increases: 93% in female mice, p=0.0021, and 67% in male mice, p=0.0018) (Figure 6B). Besides the survival assessment, we also employed a cohort of mice (three per treatment group) to examine the tumor growth in major organs at the end of treatment. Compared to control groups, palbociclib treatment at 100 mg/kg as a single agent, significantly decreased tumor burden in visceral organs, especially in the liver, along with a marked reduction in MYC expression. However, residual tumor cells remain conspicuously present, especially along blood vessels. While gemcitabine monotherapy induced less significant tumor reduction compared to palbociclib, the combination of both marked improved therapeutic efficacy, leaving minimal residual tumor cells in various visceral organs (Figure 6C).

Discussion

Recent advances in treating ENKTL, including L-asparaginase integration, remain largely confined to conventional chemotherapy and radiotherapy. Advanced-stage ENKTL patients often face poor outcomes, with limited options for refractory or relapsed disease. While genomic studies have pinpointed key alterations in ENKTL, such as loss of *PRDM1*, *TP53,* and *FOXO3*, and gain-of-function mutations in the JAK/STAT pathway,[4, 7, 9, 27, 28] direct targeting of these drivers remains challenging in the clinical management of this disease. This study shifts focus to MYC, a critical oncogene in hematologic malignancies, investigating its therapeutic implications. Surprisingly, approximately three-quarters of the investigated ENKTL cases showed MYC overexpression, with few genetic alterations, aligning with the fact that MYC is downstream of multiple drivers in ENKTL.[7, 9] Notably, MYC overexpression was more pronounced in most of the relapsed ENKTL cases. Coupled with findings from our *in vivo* study showing that gemcitabine treatment alone had little impact on the MYC expression, it raises a question of whether MYC also participated in the treatment resistance of ENKTL, especially given that some relevant mechanisms for this have been identified in pancreatic cancer.[29, 30]

Cancer prognostic models are valuable tools to improve the management of patients by providing risk stratification. For ENKTL, the recently developed PINK

prognostic model consists of four independent risk factors: age >60 years, stage III/IV disease, distant lymph node metastasis, and non-nasal-type disease. PINK-E, which further integrates detectable plalsma EBV DNA, is now commonly used in clinical practice. Nevertheless, since most patients present with localized or early-stage disease at diagnosis, they are likely to be stratified as low-risk by the PINK/PINK-E indexes. However, in some of the low-risk patients, the clinical outcomes were not as good as expected with standard treatment. This issue has been noticed repeatedly in previous studies,[31, 32] and also was found in our study. In particular, we observed two notable declines in the survival curve for the low-risk group stratified by PINK-E, one within the first 2 years and the other 5 years after the diagnosis. This finding suggests that PINK/PINK-E stratification may fail to identify a subset of patients at higher risk of refractory or relapse. We speculated one major reason for this deficiency is the lack of biological indicators. Indeed, when either MYC expression or Ki-67 index was incorporated into the prognostic model, it significantly improved the discrimination with a substantial proportion of the cases being removed from the low-risk group. These two new models have their own advantages. The PINK-EK exhibited better discrimination for the low-risk group, whereas the PINK-EM outperformed in identifying high-risk cases. Further validations on a larger scale are required to evaluate their efficacy and determine which one would be more useful in clinical practice.

Given the important role of MYC in cancer development, considerable efforts have been dedicated to targeting it in cancer cells. However, to date, no direct targeting strategies have received clinical approval for application. In this study, we adopted an alternative strategy to target MYC downstream genes that are essential for its function in ENKTL cells. We considered CDK4 and HK2 as potential targets, not only because they are the key regulators of their respective pathways which are crucial for MYC function, but also because both are kinases that could be targeted by small molecule inhibitors. Our focus turned to CDK4, primarily because CDK4/6 inhibitors have been extensively tested in clinical trials for various types of cancers and have been approved for the treatment of breast cancer. However, as a canonical MYC target with an emerging role in cancer treatment,[33] HK2 holds considerable promise in the treatment of MYC-associated malignancies, especially given the recent advances in identifying potent and selective HK2 inhibitors.[34] Since MYC aberration is frequently observed in many types of cancers, it raises the possibility that CDK4 inhibition may also be efficacious in other cancers where MYC plays a significant role. An affirmative answer might be supported by the fact that CDK4 is a classic MYC target and there is a significant overlap between MYC and E2F bound genes.[35, 36] Nevertheless, given that transcriptional regulation is a highly dynamic mechanism orchestrated by a large number of molecules, the impact of MYC on a gene is greatly dependent on the specific context of the cell. Besides, the contribution of the target gene to tumor biology and compensatory mechanisms upon inhibition are also important factors determining the therapeutic efficacy. Therefore, CDK4 inhibition as a treatment for MYC-associated malignancies needs to be specifically investigated in different cancers. Surprisingly, palbociclib treatment induced substantial MYC depletion in the NK malignancy models,

both *in vitro* and *in vivo*, which might be an important underlying mechanism contributing to the effectiveness of the treatment. We speculate that this is mainly through transcription reprogramming upon RB activation, which also implies that the active proliferative status mediated by E2F is a prerequisite for MYC overexpression in NK malignancy cells (Figure 5E). Notably, genetic aberrations of the RB gene were barely identified in this disease, further highlighting the potential of this treatment strategy. One notable limitation is the predominant use of IMC-1 and NK-92 cells in the functional study. While these cells exhibit exceptionally high MYC expression, they are not derived from typical ENKTL patients and may not fully capture the diverse cellular characteristics of ENKTL. In the xenograft experiments, although the treatment did not eradicate the tumor and all mice eventually died from the outgrowth of tumor cells after treatment was discontinued, palbociclib exhibited a potent anti-tumor effect, especially when combined with gemcitabine. Given the challenges of tracking tumor growth in visceral organs, our treatments were limited to a three-week period, followed by a survival assessment. We speculate that additional cycles of treatment and a more strategically optimized drug combination may further improve therapeutic efficacy.

In conclusion, our findings underscored that MYC, despite not being a primary driver, is an oncogene with prognostic significance in ENKTL, and can serve as a biomarker to evaluate the aggressiveness of the tumor. Further, we demonstrated that the clinical-grade CDK4/6 inhibitor palbociclib is promising in the treatment of ENKTL with MYC overexpression. Clinical trials are desired to further determine the safety and efficacy of this treatment approach in patients with ENKTL.

References

1. Lee J, Suh C, Park YH, et al. Extranodal natural killer T-cell lymphoma, nasal-type: a prognostic model from a retrospective multicenter study. J Clin Oncol. 2006;24(4):612-618.
2. Au WY, Weisenburger DD, Intragumtornchai T, et al. Clinical differences between nasal and extranasal natural killer/T-cell lymphoma: a study of 136 cases from the International Peripheral T-Cell Lymphoma Project. Blood. 2009;113(17):3931-3937.
3. Kommalapati A, Tella SH, Ganti AK, Armitage JO. Natural Killer/T-cell Neoplasms: Analysis of Incidence, Patient Characteristics, and Survival Outcomes in the United States. Clin Lymphoma Myeloma Leuk. 2018;18(7):475-479.
4. Kucuk C, Iqbal J, Hu X, et al. PRDM1 is a tumor suppressor gene in natural killer cell malignancies. Proc Natl Acad Sci U S A. 2011;108(50):20119-20124.
5. Iqbal J, Wright G, Wang C, et al. Gene expression signatures delineate biological and prognostic subgroups in peripheral T-cell lymphoma. Blood. 2014;123(19):2915-2923.
6. Kucuk C, Hu X, Jiang B, et al. Global promoter methylation analysis reveals novel candidate tumor suppressor genes in natural killer cell lymphoma. Clin Cancer Res. 2015;21(7):1699-1711.
7. Kucuk C, Jiang B, Hu X, et al. Activating mutations of STAT5B and STAT3 in lymphomas derived from gammadelta-T or NK cells. Nat Commun. 2015;6:6025.
8. Selvarajan V, Osato M, Nah GSS, et al. RUNX3 is oncogenic in natural killer/T-cell lymphoma and is transcriptionally regulated by MYC. Leukemia. 2017;31(10):2219-2227.
9. Xiong J, Cui BW, Wang N, et al. Genomic and Transcriptomic Characterization of Natural Killer T Cell Lymphoma. Cancer Cell. 2020;37(3):403-419.
10. Dong G, Li Y, Lee L, et al. Genetic manipulation of primary human natural killer cells to investigate the functional and oncogenic roles of PRDM1. Haematologica. 2021;106(9):2427-2438.
11. Meyer N, Penn LZ. Reflecting on 25 years with MYC. Nat Rev Cancer. 2008;8(12):976-990.
12. de Mel S, Hue SS, Jeyasekharan AD, Chng WJ, Ng SB. Molecular pathogenic pathways in extranodal NK/T cell lymphoma. J Hematol Oncol. 2019;12(1):33.
13. Kiuchi N, Nakajima K, Ichiba M, et al. STAT3 is required for the gp130-mediated full activation of the c-myc gene. J Exp Med. 1999;189(1):63-73.
14. Pinz S, Unser S, Rascle A. Signal transducer and activator of transcription STAT5 is recruited to c-Myc super-enhancer. BMC Mol Biol. 2016;17:10.
15. Wingelhofer B, Neubauer HA, Valent P, et al. Implications of STAT3 and STAT5 signaling on gene regulation and chromatin remodeling in hematopoietic cancer. Leukemia. 2018;32(8):1713-1726.
16. Horsley V, O'Carroll D, Tooze R, et al. Blimp1 defines a progenitor population that governs cellular input to the sebaceous gland. Cell. 2006;126(3):597-609.
17. Yu L, Yu TT, Young KH. Cross-talk between Myc and p53 in B-cell lymphomas. Chronic Dis Transl Med. 2019;5(3):139-154.
18. Huang X, Sun Q, Fu H, Zhou X, Guan X, Wang J. Both c-Myc and Ki-67 expression are predictive markers in patients with extranodal NK/T-cell lymphoma, nasal type: a retrospective study in China. Pathol Res Pract. 2014;210(6):351-356.
19. Wang JH, Bi XW, Li PF, et al. Overexpression of MYC and BCL2 Predicts Poor Prognosis in Patients with Extranodal NK/T-cell Lymphoma, Nasal Type. J Cancer. 2017;8(5):793-800.
20. Swerdlow SH CE, Harris NL, Jaffe ES, Pileri SA, Stein H. WHO Classification of Tumors of Haematopoietic and Lymphoid Tissues. Vol. 4, revised ed: International Agency for Research on Cancer, 2017.
21. Lin N, Song Y, Zheng W, et al. A prospective phase II study of L-asparaginase- CHOP plus radiation in newly diagnosed extranodal NK/T-cell lymphoma, nasal type. J Hematol Oncol. 2013;6:44.

22. Kim SJ, Yoon DH, Jaccard A, et al. A prognostic index for natural killer cell lymphoma after non-anthracycline-based treatment: a multicentre, retrospective analysis. Lancet Oncol. 2016;17(3):389-400.
23. Hong H, Li Y, Lim ST, et al. A proposal for a new staging system for extranodal natural killer T-cell lymphoma: a multicenter study from China and Asia Lymphoma Study Group. Leukemia. 2020;34(8):2243-2248.
24. Kim JW, Zeller KI, Wang Y, et al. Evaluation of myc E-box phylogenetic footprints in glycolytic genes by chromatin immunoprecipitation assays. Mol Cell Biol. 2004;24(13):5923-5936.
25. Hermeking H, Rago C, Schuhmacher M, et al. Identification of CDK4 as a target of c-MYC. Proc Natl Acad Sci U S A. 2000;97(5):2229-2234.
26. Li W, Zheng M, Wu S, et al. Benserazide, a dopadecarboxylase inhibitor, suppresses tumor growth by targeting hexokinase 2. J Exp Clin Cancer Res. 2017;36(1):58.
27. Karube K, Nakagawa M, Tsuzuki S, et al. Identification of FOXO3 and PRDM1 as tumor-suppressor gene candidates in NK-cell neoplasms by genomic and functional analyses. Blood. 2011;118(12):3195-3204.
28. Koo GC, Tan SY, Tang T, et al. Janus kinase 3-activating mutations identified in natural killer/T-cell lymphoma. Cancer Discov. 2012;2(7):591-597.
29. Farrell AS, Joly MM, Allen-Petersen BL, et al. MYC regulates ductal-neuroendocrine lineage plasticity in pancreatic ductal adenocarcinoma associated with poor outcome and chemoresistance. Nat Commun. 2017;8(1):1728.
30. Ganguly K, Bhatia R, Rauth S, et al. Mucin 5AC Serves as the Nexus for beta-Catenin/c-Myc Interplay to Promote Glutamine Dependency During Pancreatic Cancer Chemoresistance. Gastroenterology. 2022;162(1):253-268.
31. Hong H, Huang H, Fang X, et al. A prognostic index for nasal-type early-stage extranodal natural killer/T-cell lymphoma: A multicenter study. Am J Hematol. 2019;94(5):E122-E124.
32. Chen SY, Yang Y, Qi SN, et al. Validation of nomogram-revised risk index and comparison with other models for extranodal nasal-type NK/T-cell lymphoma in the modern chemotherapy era: indication for prognostication and clinical decision-making. Leukemia. 2021;35(1):130-142.
33. Stine ZE, Schug ZT, Salvino JM, Dang CV. Targeting cancer metabolism in the era of precision oncology. Nat Rev Drug Discov. 2022;21(2):141-162.
34. Zheng M, Wu C, Yang K, et al. Novel selective hexokinase 2 inhibitor Benitrobenrazide blocks cancer cells growth by targeting glycolysis. Pharmacol Res. 2021;164:105367.
35. Li Z, Van Calcar S, Qu C, Cavenee WK, Zhang MQ, Ren B. A global transcriptional regulatory role for c-Myc in Burkitt's lymphoma cells. Proc Natl Acad Sci U S A. 2003;100(14):8164-8169.
36. Zeller KI, Zhao X, Lee CW, et al. Global mapping of c-Myc binding sites and target gene networks in human B cells. Proc Natl Acad Sci U S A. 2006;103(47):17834-17839.

Table 1. The baseline characteristics and therapeutic approaches for this cohort of patients (N = 111)

Variables	n (%)
Age (≤60)	103 (92.8)
Male	74 (66.7)
ECOG performance	
<2	99 (89.2)
≥2	12 (10.8)
Ann Arbor staging	
I-II	85 (76.6)
III-IV	26 (23.4)
B symptoms	
No	57 (51.3)
Yes	54 (48.6)
Primary site	
UAT	91 (82.0)
*Non-UAT**	20 (18.0)
PTI	
No	64 (57.7)
Yes	47 (42.3)
Regional LN involvement	
Absent	62 (55.9)
Present	49 (44.1)
Distant organ metastasis	
No	92 (82.9)
Yes	19 (17.1)
Elevated LDH	28 (25.2)
Detectable EBV-DNA	84 (75.7)
PINK-E score	
<2	85 (76.6)
≥2	26 (23.4)
Primary treatment	
Chemotherapy	42 (37.8)
CMT[#]	69 (62.2)
Chemotherapy regimen	
Peg/Asp -based	86 (77.5)
Anthracyclines-based	21 (18.9)
Others	4 (3.6)

#Combinational modality treatment (CMT) indicates the combination of radiotherapy and chemotherapy.

*Non-UAT sites: 9 in skin and soft tissues; 4 in the testis/suprarenal gland; 3 in the intestine; 4 in other sites.

Abbreviations: Asp, Asparaginase; CMT, Combinational modality treatment; ECOG, Eastern Cooperative Oncology Group; LDH, Lactate dehydrogenase; LN, Lymph node; PTI, Primary tumor invasion; Peg, Pegaspargase; PINK-E, Prognostic index for natural killer cell lymphoma-EBV; UAT, Upper aerodigestive tract.

Figure Legends:

Figure 1. Overexpression of MYC in ENKTL cases. (A) H&E and IHC staining for MYC and Ki-67 are shown in a representative case of MYC-Low and MYC-High ENKTL. (B) Summary of MYC and Ki-67 positivity in this cohort of cases. (C) The correlation between MYC and Ki-67 in this cohort of cases. (D) Comparison of MYC-positive percentages between diagnostic and relapsed samples in 18 paired cases. (E) Two representative cases showing a remarkable upregulation of MYC expression in the relapsed samples.

Figure 2. MYC overexpression as a prognostic marker in ENKTL. (A-B) The PFS (A) and OS (B) curves for the cohort, categorized by MYC expression. PFS: median 50.4 months (95% CI 39.1-60.7) vs. median 78.3 months (95% CI 50.1-86.1); OS: median 60.6 months (95% CI 48.9-70.5) vs. median 72.5 months (95% CI 57.8-89.6). (C-D) The cases were stratified by PINK-E model, and the PFS (C) and OS (D) curves are shown for each group. (E-F) The cases were stratified by the PINK-EM model which integrates PINK-E and MYC overexpression, and the PFS (E) and OS (F) curves are shown for each group. (G-H) The cases were stratified by the PINK-EK model which integrates PINK-E and Ki-67 index, and the PFS (G) and OS (H) curves are shown for each group.

Figure 3. MYC KD decreased the viability of NK malignancy cells. (A-B) The mRNA and protein levels of MYC in seven NK malignancy cell lines as measured by qRT-PCR (A) and WB (B). (C) MYC KD in NK-92 and IMC-1 cells with the protein levels measured by WB. Three siRNA mixtures, annotated S1, S2, and S3 were tested. (D) The cell viability was measured 72 hours after MYC KD in NK-92 and IMC-1 cells. The assay was performed in triplicate and the average values (AVs) with standard deviation (SD) are shown. (E) Cell apoptosis was determined by Annexin V and PI staining followed by flow cytometry assay after 48 hours of MYC KD. The experiments were performed in duplicates and representative density plots with AVs and SD were shown.

Figure 4. Identification of highly confident MYC targets in ENKTL. (A) The Heatmap of DEGs between the MYC-high and MYC-low ENKTL cases (n=15/group). (B) Relative MYC mRNA level between MYC-high and MYC-low groups. (C-D) The DEGs from the analysis of the primary cases were cross-compared with the commonly altered genes in NK-92 and IMC-1 cells with MYC KD. (C) The Venn diagrams show the relationship between the two sets of genes and (D) the heatmap shows the expression level of the overlapped genes in the MYC KD experiment. (E) KHYG-1, NK-92, and IMC-1 cells were knocked down with MYC for 48h and examined with MYC, HK2, and CDK4 by WB. The experiments were performed in triplicates and exhibited by a representative one.

Figure 5. Palbociclib treatment selectively inhibited NK malignancy cells with MYC overexpression. (A) NK malignancy cell lines were treated with increasing doses of palbociclib for 72h and examined with cell viability by prestoblue assay. The cell lines were ranked by the area under curve (AUC) of the inhibition plot. (B) SNK6, KHYG-1,

NK-92, and IMC-1 cells were treated with palbociclib and measured with cell cycle after 24h of treatment (upper) and apoptosis after 48h of treatment (lower). (C) SNK-6, KHYG-1, NK-92, and IMC-1 cells were treated with Palbociclib in a time-dependent manner and the CDK4 signaling and MYC levels were examined by WB. (D) Rb was knocked down by siRNA in NK-92 and IMC-1 cells for 24h, and then treated with palbociclib for 48h. Rb and MYC protein levels were measured by WB. The quantitation was carried out by analyzing the signal pixel-intensity of MYC with actin normalization. (E) Sketch illustration of the MYC-CDK4 regulation loop in NK cell malignancy.

Figure 6. Palbociclib treatment repressed tumor growth in xenograft models of NK cell malignancy with MYC overexpression. IMC-1-CDX and an ENKTL-PDX model were established in NSG mice. (A) For the IMC-1 CDX, the mice were treated with saline control (Ctrl, n=6) or palbociclib isethionate (P, n=6) daily, and monitored with survival time. (B-C) For the ENKTL-PDX, the treatment effect was investigated in female and male cohorts separately, and in each cohort, a saline control (Ctrl, n=8) and four drug treatment groups (n=8/group), including palbociclib isethionate (P) and gemcitabine hydrochloride (G), single and combined treatment, were examined. (B) The survival curve for the five treatment groups (n=5/each group) of the PDX model in the female and male cohorts, respectively. (C) Three mice from each group in every cohort were euthanized immediately after the treatment concluded (on day 21 of treatment) and examined with the key organs by pathological staining. The figure shows the tumor involvement in the liver upon different treatments (magnification 40X and 400X). For each representative case, the same area is shown for different staining. (A) and (B) blue triangles indicate treatment start and orange triangles indicate treatment end.

Figure 1

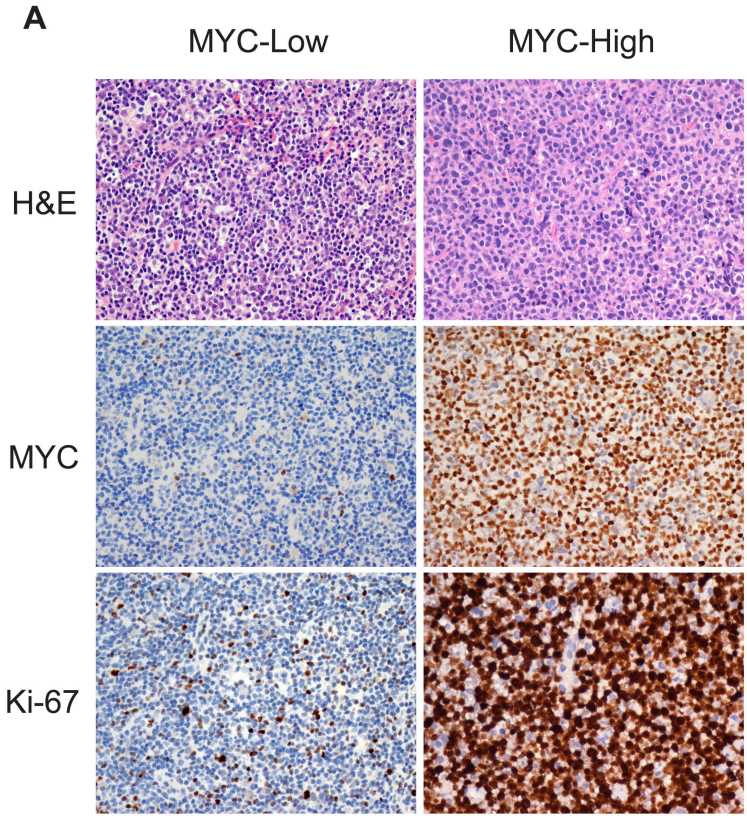

B

	MYC-Low	MYC-High
Ki-67-Low	27 (57.4%)	20 (42.6%)
Ki-67-High	1 (1.6%)	63 (98.4%)
Total	28 (25.2%)	83 (74.8%)

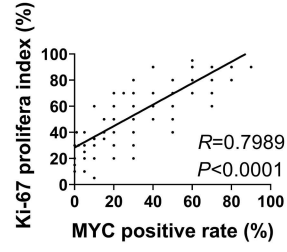

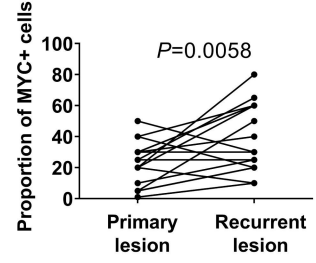

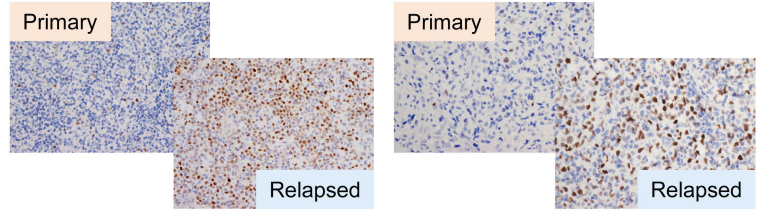

Figure 2

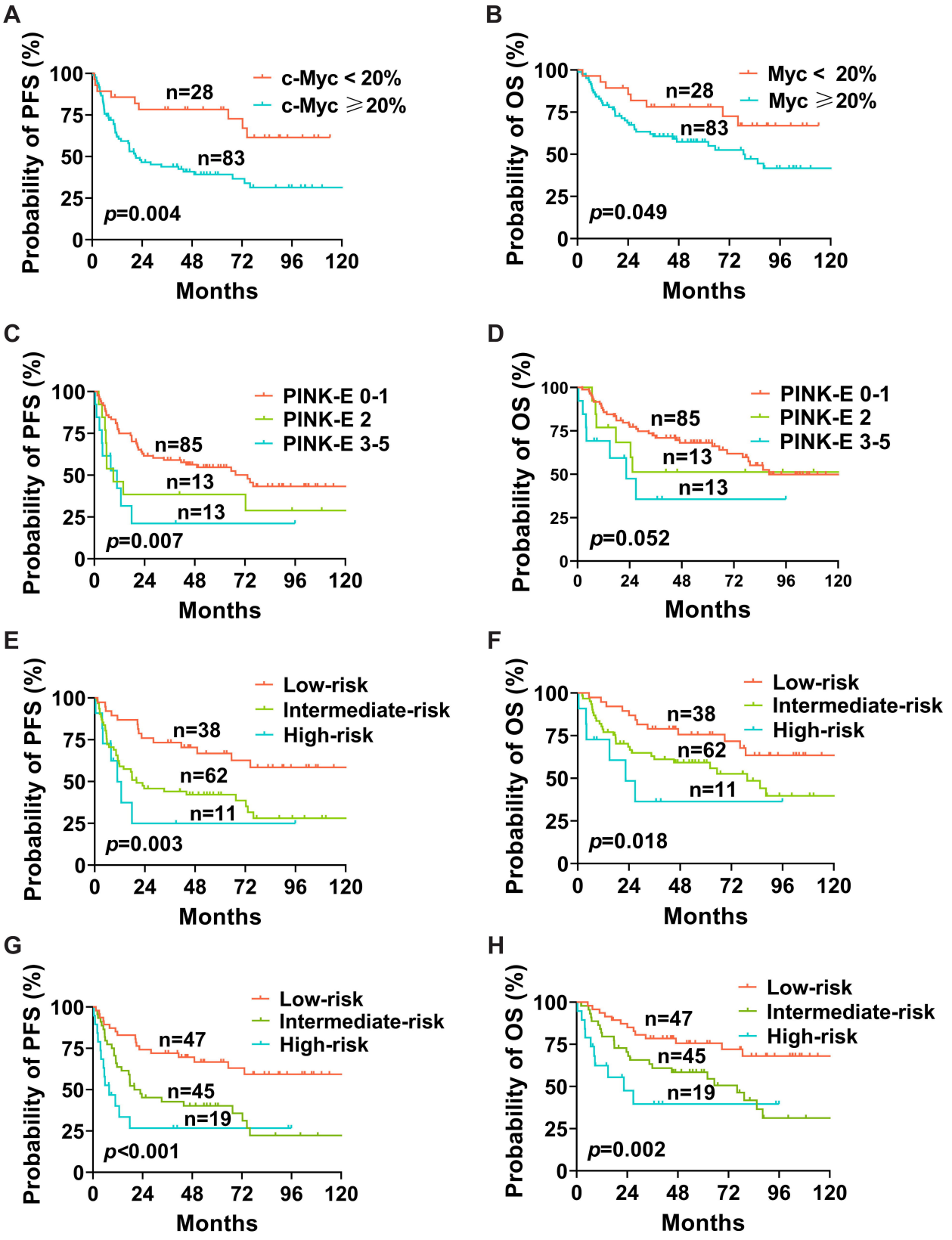
A
Probability of PFS (%)
100
75
50
25
0
0
24
48
72
96
120
Months
c-Myc < 20%
c-Myc ⩾20%
n=28
n=83
p=0.004
B
Probability of OS (%)
Myc < 20%
Myc ⩾20%
n=28
n=83
p=0.049
C
Probability of PFS (%)
PINK-E 0-1
PINK-E 2
PINK-E 3-5
n=85
n=13
n=13
p=0.007
D
Probability of OS (%)
PINK-E 0-1
PINK-E 2
PINK-E 3-5
n=85
n=13
n=13
p=0.052
E
Probability of PFS (%)
Low-risk
Intermediate-risk
High-risk
n=38
n=62
n=11
p=0.003
F
Probability of OS (%)
Low-risk
Intermediate-risk
High-risk
n=38
n=62
n=11
p=0.018
G
Probability of PFS (%)
Low-risk
Intermediate-risk
High-risk
n=47
n=45
n=19
p<0.001
H
Probability of OS (%)
Low-risk
Intermediate-risk
High-risk
n=47
n=45
n=19
p=0.002

Figure 3

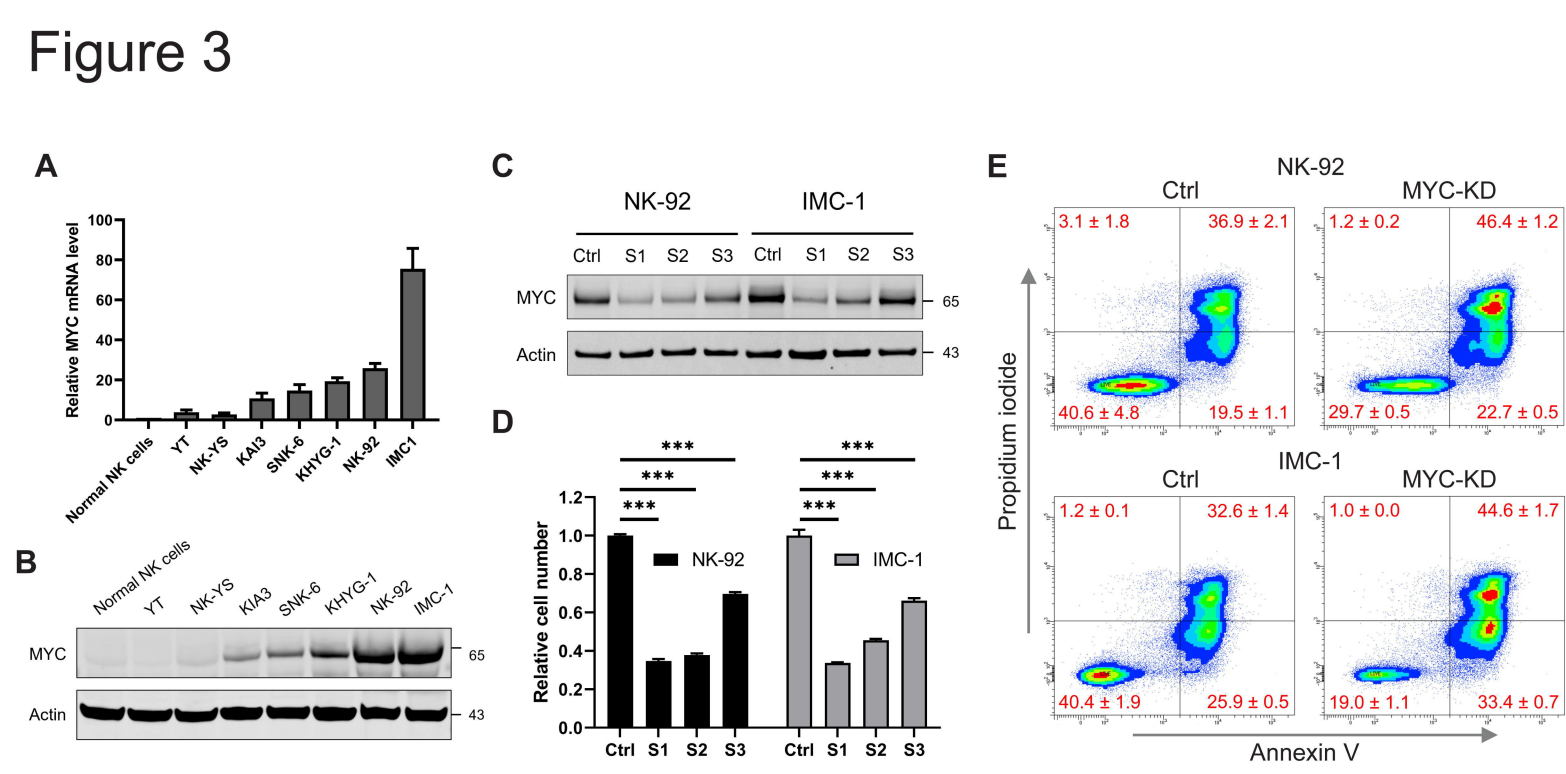
A
Relative MYC mRNA level
100
80
60
40
20
0
Normal NK cells
YT
NK-YS
KAI3
SNK-6
KHYG-1
NK-92
IMC1
B
Normal NK cells
YT
NK-YS
KIA3
SNK-6
KHYG-1
NK-92
IMC-1
MYC
65
Actin
43
C
NK-92
IMC-1
Ctrl
S1
S2
S3
Ctrl
S1
S2
S3
MYC
65
Actin
43
D
***
***
***
***
***
***
Relative cell number
1.2
1.0
0.8
0.6
0.4
0.2
0.0
NK-92
IMC-1
Ctrl
S1
S2
S3
Ctrl
S1
S2
S3
E
NK-92
Ctrl
MYC-KD
3.1 ± 1.8
36.9 ± 2.1
40.6 ± 4.8
19.5 ± 1.1
1.2 ± 0.2
46.4 ± 1.2
29.7 ± 0.5
22.7 ± 0.5
IMC-1
Ctrl
MYC-KD
1.2 ± 0.1
32.6 ± 1.4
40.4 ± 1.9
25.9 ± 0.5
1.0 ± 0.0
44.6 ± 1.7
19.0 ± 1.1
33.4 ± 0.7
Propidium iodide
Annexin V

Figure 4

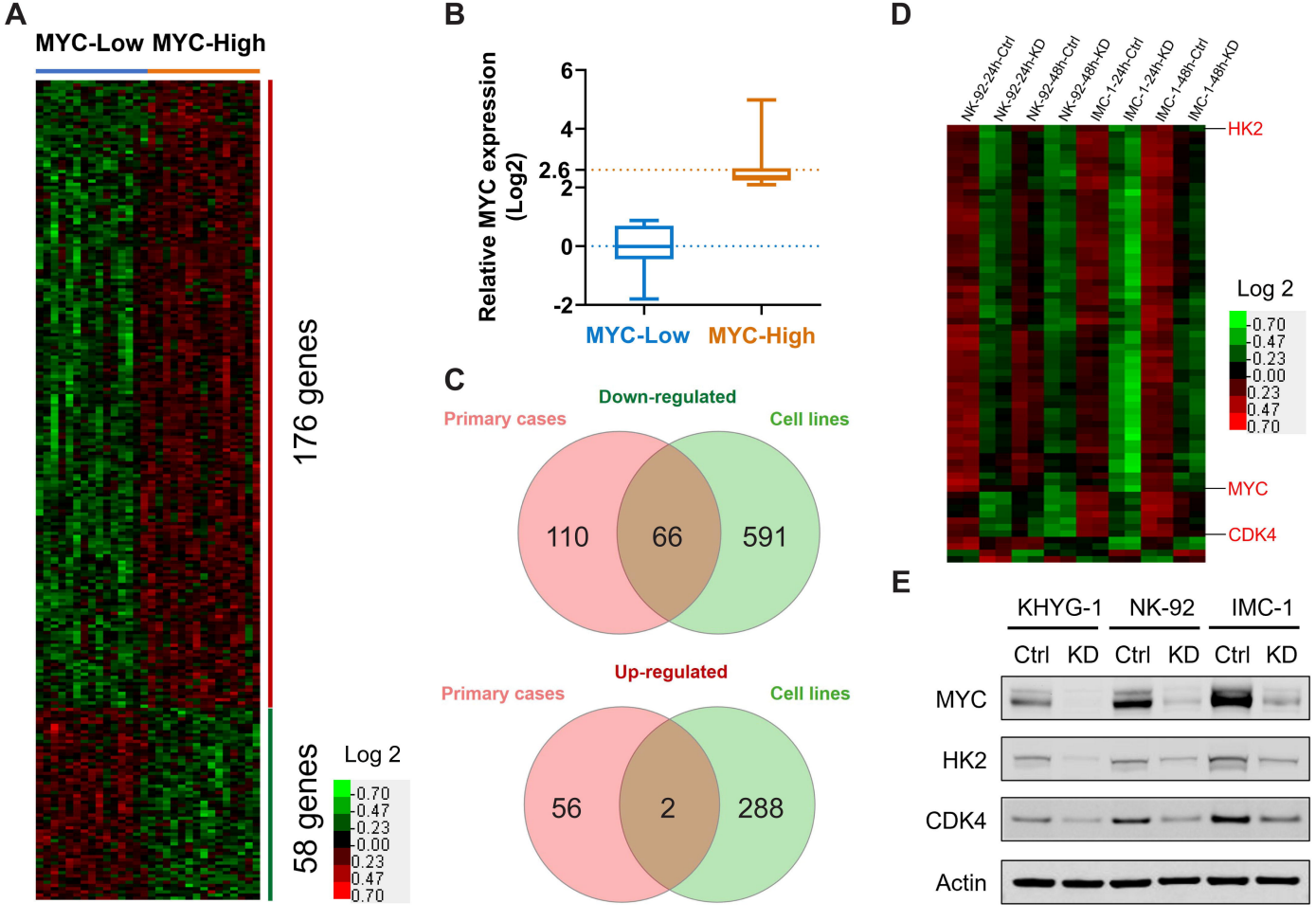
A
MYC-Low MYC-High
176 genes
58 genes
Log 2
0.70
0.47
0.23
0.00
0.23
0.47
0.70
B
Relative MYC expression (Log2)
6
4
2.6
2
0
-2
MYC-Low
MYC-High
C
Down-regulated
Primary cases
Cell lines
110
66
591
Up-regulated
Primary cases
Cell lines
56
2
288
D
NK-92-24h-Ctrl
NK-92-24h-KD
NK-92-48h-Ctrl
NK-92-48h-KD
IMC-1-24h-Ctrl
IMC-1-24h-KD
IMC-1-48h-Ctrl
IMC-1-48h-KD
HK2
Log 2
0.70
0.47
0.23
0.00
0.23
0.47
0.70
MYC
CDK4
E
KHYG-1
NK-92
IMC-1
Ctrl
KD
Ctrl
KD
Ctrl
KD
MYC
HK2
CDK4
Actin

Figure 5

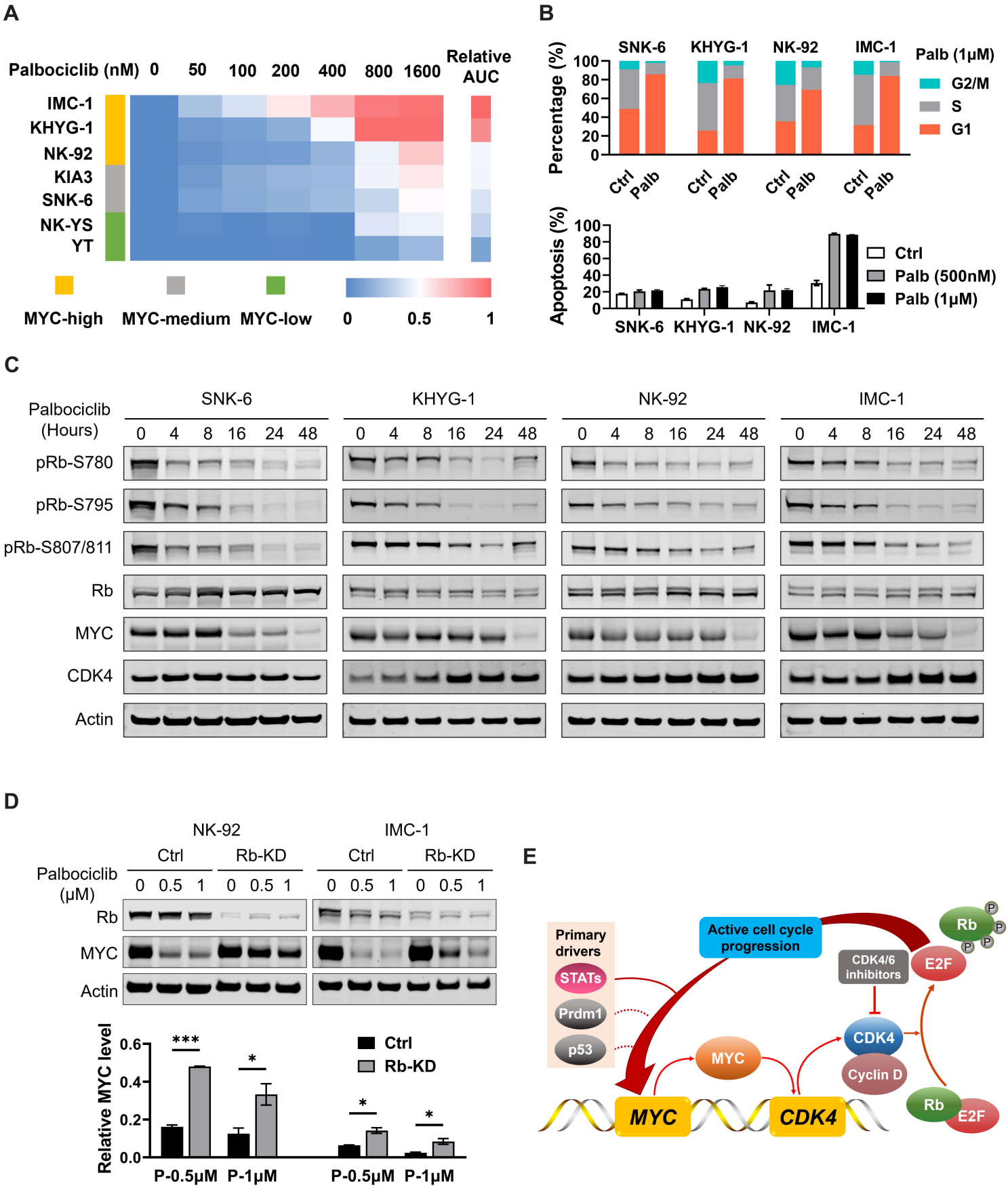
A
Palbociclib (nM) 0 50 100 200 400 800 1600
Relative AUC
IMC-1
KHYG-1
NK-92
KIA3
SNK-6
NK-YS
YT
MYC-high
MYC-medium
MYC-low
0
0.5
1
B
SNK-6
KHYG-1
NK-92
IMC-1
Palb (1μM)
G2/M
S
G1
Percentage (%)
Ctrl
Palb
Apoptosis (%)
Ctrl
Palb (500nM)
Palb (1μM)
C
Palbociclib (Hours)
0 4 8 16 24 48
pRb-S780
pRb-S795
pRb-S807/811
Rb
MYC
CDK4
Actin
D
NK-92
IMC-1
Ctrl
Rb-KD
Palbociclib (μM)
0 0.5 1
Rb
MYC
Actin
Relative MYC level
***
*
Ctrl
Rb-KD
P-0.5μM
P-1μM
E
Primary drivers
STATs
Prdm1
p53
Active cell cycle progression
CDK4/6 inhibitors
E2F
Rb
MYC
CDK4
Cyclin D
MYC
CDK4
Rb
E2F

Figure 6

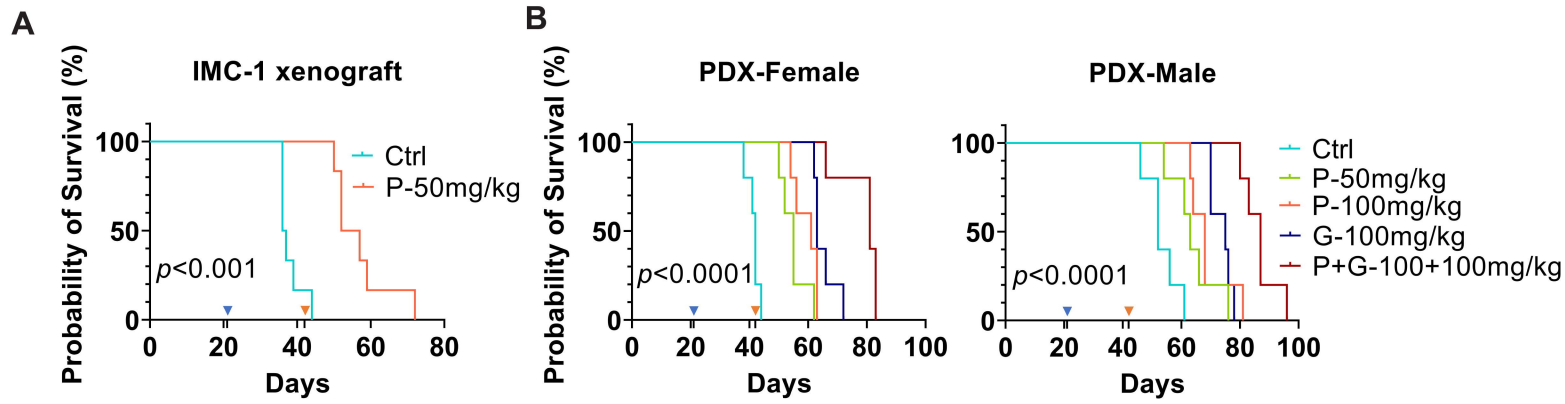
A
IMC-1 xenograft
Probability of Survival (%)
100
50
0
p<0.001
Ctrl
P-50mg/kg
0
20
40
60
80
Days
B
PDX-Female
Probability of Survival (%)
p<0.0001
0
20
40
60
80
100
Days
PDX-Male
p<0.0001
Ctrl
P-50mg/kg
P-100mg/kg
G-100mg/kg
P+G-100+100mg/kg

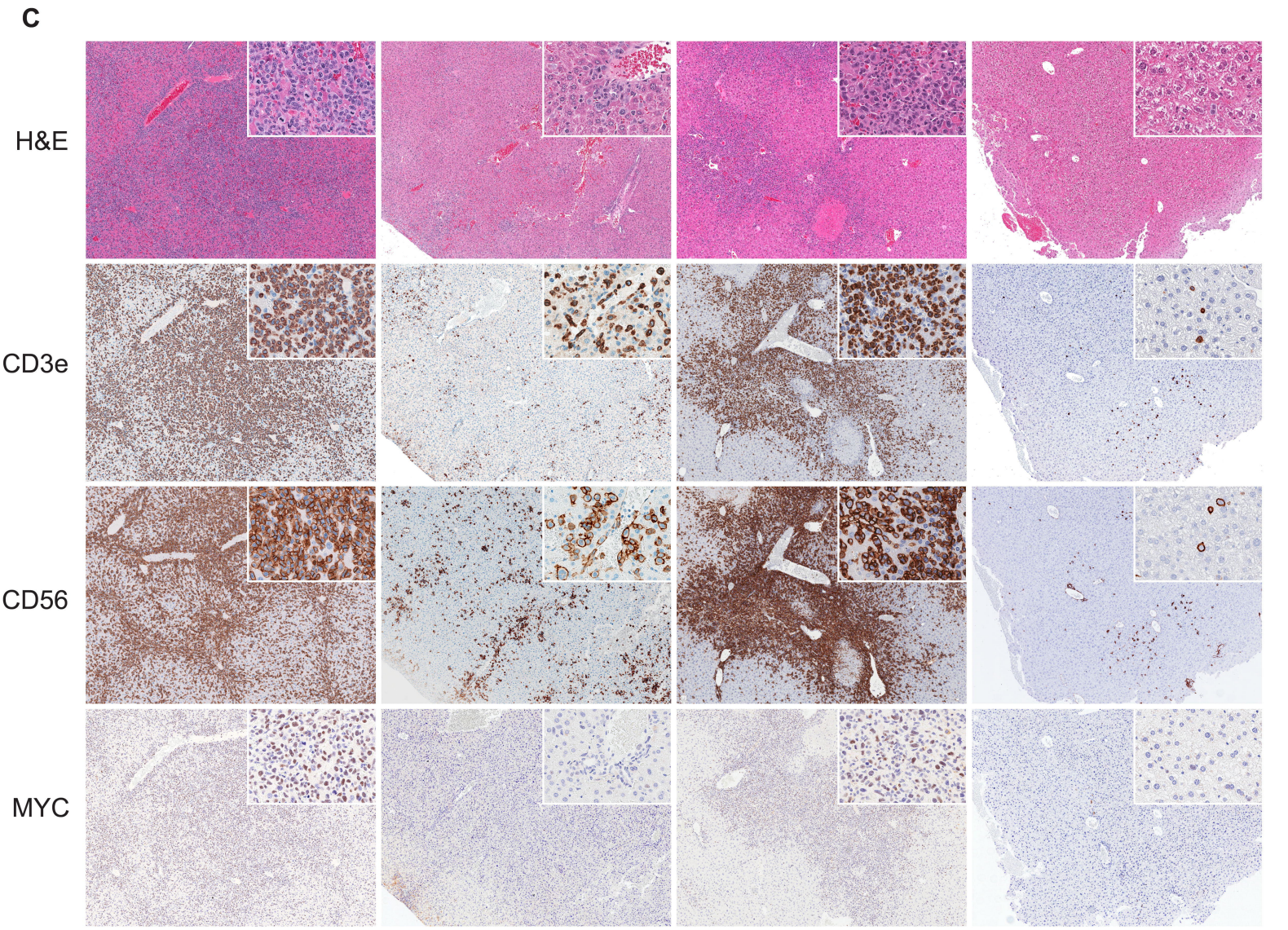
C
H&E
CD3e
CD56
MYC
Ctrl
P-100 mg/kg
G-100mg/kg
P-100mg/kg
G-100mg/kg

Supplementary Materials and Methods

Cell culture

The cell lines included in this study have been described previously.[1,2] All cell lines were cultured in RPMI 1640 medium supplemented with 15% Fetal Bovine Serum (FBS), 1% Penicillin-Streptomycin (Thermo Fisher Scientific), and 10ng/mL IL-2 (STEMCELL Technologies, Vancouver, BC, Canada). Primary normal NK cells were isolated from fresh healthy human tonsil using the human NK cell isolation kit (Miltenyi Biotec, Gaithersburg, MD, USA) and cultured in RPMI 1640 supplemented with 20% FBS, and 10 ng/mL IL-2.

Cell viability and cell cycle Assays

Cell viability was measured by using the PrestoBlue™ Cell Viability Reagent (Thermo Fisher Scientific Waltham, MA, USA). Relative fluorescence units were detected by Infinite M200 Pro plate reader (Tencan, Männedorf, Switzerland). To measure cell apoptosis, treated cells were stained by using FITC Annexin V Apoptosis Detection Kit (BD Biosciences, Franklin Lakes, NJ, USA) and detected by flow cytometry. For the cell cycle analysis, the experimental cells were fixed by cold 75% ethanol and stained by Propidium iodide (Sigma-Aldrich, St. Louis, MO, USA), followed with flow cytometry detection.

Quantitative real-time PCR

RNA was isolated by RNeasy Mini Kit (Qiagen, Germantown, MD, USA), and reversely transcribed to cDNA by using ProtoScript II First Strand cDNA Synthesis Kit (New England Biolabs, Ipswich, MA, USA). The real-time quantitative PCR was performed on Bio-Rad CFX96 Real-Time PCR Detection System(Bio-Rad) using the DyNAmo Flash SYBR Green qPCR Kit (Thermo Fisher Scientific, Waltham, MA, USA). Relative expression fold change was calculated by $2^{-\Delta\Delta CT}$ method. GAPDH was used as the housekeeping gene. PCR primers used were listed in Supplementary Table S1.

Western blot (WB)

The protein was isolated by using M-PER™ Mammalian Protein Extraction Reagent (Thermo Fisher Scientific, Waltham, MA, USA) supplied with Halt™ Protease and Phosphatase Inhibitor Cocktail (Thermo Fisher Scientific, Waltham, MA, USA). Isolated protein was denatured for 10 mins at 70°C in NuPAGE LDS Sample Buffer with reducing buffer (Thermo Fisher Scientific, Waltham, MA, USA). Protein electrophoresis was performed using Bolt 4~12% Bis-Tris Plus Gels and MES SDS running buffer (Thermo Fisher Scientific, Waltham, MA, USA). Proteins were then transferred onto nitrocellulose membrane, blocked with Odyssey TBS Blocking Buffer (LI-COR, Lincoln, NE, USA), and incubated with primary antibody overnight at 4°C. The membrane was washed and incubated with the secondary antibody for 1h at room temperature. After washing, the membrane was scanned on the Odyssey CLx imager (LI-COR). Protein

was quantified based on band intensity using the Image Studio software (LI-COR). Protein expression change was evaluated by normalizing with β-actin or target protein input. The primary antibodies used for immunoblotting are listed in Supplementary Table S2.

Double thymidine block

In cell lines with fresh culture medium, thymidine (Sigma-Aldrich, St. Louis, MO, USA) was added at a final concentration of 2mM and incubated at 37 °C for 18h. Then, the cells were washed with dPBS and cultured with fresh medium at 37 °C for 9h followed by the second round of thymidine treatment at 2mM for another 18h. The cells were then subjected to downstream examination.

Immunohistochemistry (IHC)

Sections from individual formalin-fixed, paraffin-embedded (FFPE) tissues or tissue micro-arrays (TMAs) were stained automatically by BOND-MAX Autostainer (Leica Biosystems, Wetzlar, Germany) according to the manufacturer's protocol. The primary antibodies used for IHC are listed in Supplementary Table S2. Photographs were taken using the Leica Aperio CS2 scanning system with 40X magnification.

Fluorescence in situ hybridization (FISH)

FISH was performed on FFPE tissues for 60 ENKTL cases. The MYC Dual Color Break Apart Rearrangement Probe and the IGH/MYC/CEP 8 Tri-Color DF FISH Probe (Vysis; Abbott Molecular, Desplaines, IL, USA) were used to interrogate the MYC locus at chromosome 8q24. and the presence of MYC translocation/amplification according to the manufacturer's protocol in the FFPE specimens, respectively.

Briefly, 3–4 μm-thick FFPE tissue sections were cut and incubated at 56°C for 3 hours. After deparaffinizing and dehydrating the sections, they were incubated in 2x saline sodium citrate buffer (2x SSC, pH 7.0) at 75°C for 20 minutes and were then digested with proteinase K (0.2 mg/mL) at 37°C for 20 minutes. Probe sets were applied onto the tissue sections on each slide followed by denaturation at 80°C for 5 minutes. Probes were then hybridized overnight at 37°C using the ThermoBrite system (Vysis). Nuclei were counterstained with 4,6-di-amidino-2-phenylindole (DAPI, Vysis) and FISH signals were assessed using an Olympus BX61 microscope (Olympus, Tokyo, Japan). Hybridization signals were assessed in 200 interphase nuclei, with an established cutoff of 15% for *MYC* rearrangement of the locus, and copy numbers >5 or the ratio of green to red signal > 2 for *MYC* amplification. Images were acquired using the BioView Automated Imaging Analysis System (BioView, Rehovot, Israel).

Statistics and data analysis

The Overall Survival (OS) and Progression-Free Survival (PFS) curves were analyzed by the Kaplan-Meier method. For the RNA sequencing, FPKM was used to estimate gene expression levels, and DESeq2 method[3] was used to analyze the differential

gene expression with the screening threshold of log2(FoldChange) ≥1 and padj ≤ 0.05. Gene expression and pathway enrichment analysis was based on the GSEA/MSigDB database. The Data from functional and animal studies were analyzed by using GraphPad Prism 9 software. Data shown with the mean ± SD are from at least two independent experiments. Unpaired t-test was used to compare data from two independent groups. One-way analysis of variance (ANOVA) was used to compare data from three or more independent groups. *P*-values of less than 0.05 were considered significant.

Reference

1. Iqbal J, Weisenburger DD, Chowdhury A, et al. Natural killer cell lymphoma shares strikingly similar molecular features with a group of non-hepatosplenic gammadelta T-cell lymphoma and is highly sensitive to a novel aurora kinase A inhibitor in vitro. *Leukemia*. 2011;25(2):348-358.
2. Kucuk C, Iqbal J, Hu X, et al. PRDM1 is a tumor suppressor gene in natural killer cell malignancies. *Proc Natl Acad Sci U S A*. 2011;108(50):20119-20124.
3. Love MI, Huber W, Anders S. Moderated estimation of fold change and dispersion for RNA-seq data with DESeq2. *Genome Biol*. 2014;15(12):550.

Supplementary Table S1. List of oligos used in this study

qRT-PCR primers		**Forward**	**Reverse**
MYC-1		GGTGCTCCATGAGGAGACA	CCTGCCTCTTTTCCACAGAA
MYC-2		GGACCCGCTTCTCTGAAAGG	TAACGTTGAGGGGCATCGTC
GAPDH		CCACTCCTCCACCTTTGAC	ACCCTGTTGCTGTAGCCA
siRNA			
MYC-S1	MYC-1	rArUrCrArUrUrGrArGrCrCrArArArUrCrUrUrArArArArAAA rUrUrUrUrUrUrUrArArGrArUrUrUrGrGrCrUrCrArArUrGrArUrArU	
	MYC-2	rGrGrArArCrGrArGrCrUrArArArArCrGrGrArGrCrUrUrUTT rArArArArArGrCrUrCrCrGrUrUrUrUrArGrCrUrCrGrUrUrCrCrUrC	
MYC-S2	MYC-3	rCrGrArCrGrArGrArCrCrUrUrCrArUrCrArArArArArCrATC rGrArUrGrUrUrUrUrUrGrArUrGrArArGrGrUrCrUrCrGrUrCrGrUrC	
	MYC-4	rArGrGrArArArArCrGrArUrUrCrCrUrUrCrUrArArCrArGAA rUrUrCrUrGrUrUrArGrArArGrGrArArUrCrGrUrUrUrUrCrCrUrUrA	
MYC-S3	MYC-5	rUrArUrArUrCrArUrUrGrArGrCrCrArArArUrCrUrUrArAAA rUrUrUrUrArArGrArUrUrUrGrGrCrUrCrArArUrGrArUrArUrArUrU	
	MYC-6	rGrArCrUrGrArArArGrArUrUrUrArGrCrCrArUrArArUrGTA rUrArCrArUrUrArUrGrGrCrUrArArArUrCrUrUrUrCrArGrUrCrUrC	
Rb-1		rGrUrArCrCrArArArGrUrUrGrArUrArArUrGrCrUrArUrGTC rGrArCrArUrArGrCrArUrUrArUrCrArArCrUrUrUrGrGrUrArCrUrG	
Rb-2		rGrGrArUrUrArUrUrGrArUrArGrUrArCrUrCrUrUrGrGrUTT rArArArCrCrArArGrArGrUrArCrUrArUrCrArArUrArArUrCrCrUrC	

Supplementary Table S2. List of antibodies used for WB and IHC

Target protein	Manufacturer	Clone	Application
MYC	Abcam	Y69	WB/IHC
HK2	Abcam	EPR20839	WB
CDK4	Cell Signaling Technology	D9G3E	WB
Rb	Thermo Fisher Scientific	1F8	WB
p-Rb (S780)	Abcam	EPR182(N)	WB
p-Rb (S795)	Cell Signaling Technology	Polyclonal	WB
p-Rb (S807/811)	Cell Signaling Technology	D20B12	WB
β-Actin	Santa Cruz	C4	WB
Ki-67	Dako	MIB-1	IHC
CD3e	Thermo Fisher Scientific	SP7	IHC
CD56	Cell Signaling Technology	E7X9M	IHC

Supplementary Table S3. Correlation between MYC expression and major clinical features in this cohort of ENKTL cases (N=111)

Characteristics		MYC		
		Low level n (%)	High level n (%)	p-value
Patients		28 (25.2)	83 (74.8)	
Age	≤60	26 (25.2)	77 (74.8)	1.000
	>60	2 (25.0)	6 (75.0)	
Gender	Male	16 (21.6)	58 (78.4)	0.216
	Female	12 (32.4)	25 (67.6)	
ECOG performance	<2	26 (26.3)	73 (73.7)	0.727
	≥2	2 (16.7)	10 (83.3)	
Ann Arbor staging	Ⅰ/Ⅱ	24 (28.2)	61 (71.8)	0.187
	Ⅲ/Ⅳ	4 (15.4)	22 (84.6)	
B symptoms	Absence	13 (22.8)	44 (77.2)	0.547
	Presence	15 (27.8)	39 (72.2)	
Primary tumor site	UAT	25 (27.5)	66 (72.5)	0.245
	Non-UAT	3 (15.0)	17 (85.0)	
PTI	No	17 (26.6)	47 (73.4)	0.705
	Yes	11 (23.4)	36 (76.6)	
Regional LN involvement	No	16 (25.8)	46 (74.2)	1.000
	Yes	12 (24.5)	37 (75.5)	
Distant organ metastasis	No	25 (27.2)	67 (72.8)	0.392
	Yes	3 (15.8)	16 (84.2)	
LDH	Normal	24 (28.9)	59 (71.1)	0.123
	Elevated	4 (14.3)	24 (85.7)	
Epstein-Barr virus DNA	Undetectable	8 (29.6)	19 (70.4)	0.545
	detectable	20 (23.8)	64 (76.2)	
PINK-E score	<2	23 (27.1)	62 (72.9)	0.421
	≥2	5 (19.2)	21 (80.8)	
Treatment mode	Chemotherapy	7 (16.7)	35 (83.3)	0.105
	CMT	21 (30.4)	48 (69.6)	
Chemotherapy regimens	Peg/Asp -based	22 (25.6)	64 (74.4)	0.986
	Anthracyclines-based	5 (23.8)	16 (76.2)	
	Others	1 (25.0)	3 (75.0)	
Treatment response	CR	22 (26.2)	62 (73.8)	0.909
	Non-CR	5 (21.7)	18 (78.3)	
	Unknown	1 (25.0)	3 (75.0)	

Abbreviations: Asp, Asparaginase; CMT, Combinational modality treatment; ECOG, Eastern Cooperative Oncology Group; LDH, Lactate dehydrogenase; LN, Lymph node; PTI, Primary tumor invasion; Peg,

Pegaspargase; PINK-E, Prognostic index for natural killer cell lymphoma-EBV; UAT, Upper aerodigestive tract.

Supplementary Table S4. Multivariate analysis of OS by the Cox proportional hazards model

Prognostic factors	Univariate analysis			Multivariate analysis		
	HR	95% CI	*P*-value	HR	95% CI	*P*-value
Age>60	——	——	0.113	——	——	——
Stage III/IV	1.999	1.066-3.748	**0.028**	——	——	——
ECOG performance status ≥2	2.741	1.276-5.886	**0.007**	3.032	1.404-6.546	**0.003**
Elevated LDH	——	——	0.093	——	——	——
Detectable Epstein-Barr virus DNA	——	——	0.217	——	——	——
Primary tumor invasion	——	——	0.105	——	——	——
Non-UAT	——	——	0.442	——	——	——
Regional LN involvement	——	——	0.247	——	——	——
Distant organ metastasis	2.106	1.071-4.144	**0.027**	——	——	——
Ki67≥65%	2.337	1.296-4.212	**0.004**	2.457	1.359-4.441	**0.005**
c-Myc≥20%	2.110	0.985-4.523	**0.049**	——	——	——

Non-UAT, non-upper aerodigestive tract; LN, Lymph node.

Supplementary Table S5. Multivariate analysis of PFS by the Cox proportional hazards model

Prognostic factors	Univariate analysis			Multivariate analysis		
	HR	95% CI	*P*-value	HR	95% CI	*P*-value
Age>60	1.10	0.40-3.05	0.847	-	-	-
Stage III/IV	2.49	1.44-4.32	0.001	1.92	0.74-4.96	0.180
ECOG performance status ≥2	1.87	0.89-3.94	0.010	1.83	0.85-3.94	0.125
Elevated LDH	1.63	0.93-2.87	0.089	1.19	0.67-2.14	0.533
Detectable Epstein-Barr virus DNA	1.40	0.76-2.59	0.281	-	-	-
Primary tumor invasion	1.03	0.61-1.73	0.903	-	-	-
Non-UAT	1.40	0.76-2.6	0.280	-	-	-
Regional LN involvement	1.25	0.75-2.07	0.396	-	-	-
Distant organ metastasis	2.38	1.30-4.35	0.005	0.98	0.34-2.82	0.970
Ki67≥65%	2.28	1.36-3.82	0.002	1.49	0.81-2.75	0.201
c-Myc≥20%	2.72	1.33-5.55	0.006	1.86	0.81-4.26	0.141

Non-UAT, non-upper aerodigestive tract; LN, Lymph node.

Supplementary Table S6. Commonly altered genes in primary case and cell line analysis

RNA-seq data Log2 transformed

Gene	NK24_C1	NK24_C2	NK24_M1	NK24_M2	NK48_C1	NK48_C2	NK48_M1	NK48_M2	IM24_C1	IM24_C2	IM24_M1	IM24_M2	IM48_C1	IM48_C2	IM48_M1	IM48_M2
HPDL	10.9993	10.8979	8.84786	9.33826	10.4654	10.1984	8.54135	9.30939	9.89395	9.66614	7.37461	6.28251	10.2985	10.3253	8.33512	8.39229
TRAP1	11.8349	11.7087	9.9496	10.239	11.654	11.3752	9.95449	10.2545	11.645	11.6569	9.63602	9.16097	12.3642	12.2898	10.6898	10.2265
RNASEH1	8.74483	8.59986	6.9649	6.92813	8.58825	7.8394	6.52609	6.85873	8.12969	7.77138	6.57115	5.73231	8.46367	8.16231	6.85064	6.30593
TTLL12	11.7561	11.5909	9.69247	9.97253	11.247	10.9011	9.79646	9.98939	12.62	12.5487	10.8746	10.5043	12.9141	12.8233	11.779	11.537
HSPD1	14.422	14.5989	12.716	13.1674	14.3198	13.9299	12.8004	12.9966	14.7191	14.7038	12.8646	11.8951	14.9769	14.9468	13.8545	13.2439
IFRD2	11.2174	11.0053	9.46465	9.66432	10.911	10.4428	9.60993	9.76722	11.9305	11.7051	9.84041	9.07724	11.9242	11.7861	10.9153	10.6128
RUVBL1	12.0931	12.0919	10.5769	10.7796	11.9422	11.5475	10.5807	10.8222	11.7178	11.5537	10.117	9.42679	12.0236	11.7976	10.6749	10.4131
HK2	11.7814	11.7493	9.83639	10.4854	11.4728	11.4428	9.91548	10.3028	11.4763	11.5131	9.71667	10.1148	11.6114	11.8959	10.7611	10.3645
SLC19A1	10.8719	10.8011	8.71492	9.22156	10.4388	9.6994	9.04564	9.33338	11.3445	11.3809	9.67136	9.11971	11.4418	11.2387	10.6351	10.4336
PRMT3	10.444	10.4312	9.15139	9.34121	10.2838	10.1173	9.19067	9.18546	10.0391	10.0128	8.39012	7.63231	10.1965	10.1888	9.15392	8.67577
FBL	12.8742	12.8221	11.0829	11.3486	12.5785	12.1713	11.2342	11.467	12.4019	12.3767	11.3169	11.1723	13.1034	12.9408	11.687	11.3879
FAM216A	9.89936	9.80913	8.23339	8.61403	9.71501	9.32943	8.24762	8.8707	10.2137	10.2781	8.62786	8.15858	10.4933	10.4735	9.45314	9.07807
EBPL	10.6636	10.6917	8.90024	8.96299	10.3057	9.72025	8.73968	9.0525	9.74671	9.50545	8.6081	7.99104	10.1172	9.97981	8.97727	8.6902
WDR74	10.3038	10.2956	8.89533	9.01928	9.877	9.27843	8.58988	8.72992	10.2175	10.1291	8.77101	8.3301	10.5548	10.2654	9.1323	9.04477
NOLC1	13.1524	13.2206	11.685	12.0188	12.9971	12.5884	11.713	12.0376	13.2399	13.3498	11.5077	10.6184	13.3655	13.3106	12.6004	12.0612
DPH5	9.77808	9.95923	8.50547	8.982	9.69367	9.61799	8.46735	8.79419	9.2111	9.26146	7.79742	7.23784	9.82555	9.5229	8.4444	8.1787
PHB	11.9133	11.8868	10.3347	10.5569	11.6384	11.0842	10.2499	10.4987	11.6009	11.4923	10.2526	9.8137	11.8839	11.7727	10.901	10.5149
MRPL4	11.0888	10.9054	9.80402	9.82664	10.7398	10.2763	9.66498	9.71671	10.8121	10.7291	9.16966	8.99642	11.3072	11.1433	10.1117	9.91105
TUFM	12.8595	12.8387	11.6366	11.7049	12.5328	12.2646	11.5333	11.7716	12.46	12.2965	10.9802	10.6537	12.9433	12.8571	11.6104	11.4115
PRMT1	13.0636	13.1134	11.4667	11.7812	12.7635	12.2994	11.5723	11.7303	12.4448	12.4106	11.1476	11.1859	12.8199	12.7235	11.7155	11.4805
PAICS	13.1813	13.2289	11.6932	12.2002	13.0356	12.7678	11.9438	12.031	13.5156	13.5048	11.8524	11.0289	13.396	13.3379	12.7617	12.3009
RCC1	12.0126	11.9906	10.4933	10.8245	11.7596	11.3258	10.5761	10.8237	12.1538	12.1931	10.8148	10.4047	12.4439	12.2563	11.5321	11.3773
IARS	12.2476	12.3135	11.092	11.4144	12.2303	12.1203	11.2141	11.3247	12.7785	12.6901	11.1292	10.5769	12.9214	12.8931	12.2769	11.6762
PFAS	10.7977	10.5278	9.83639	9.62616	10.5027	10.4086	9.58437	9.91906	10.8397	10.6336	9.19417	8.46023	11.2746	11.0141	10.1752	9.80899
HSP90AB	15.9053	15.9839	14.5715	14.8587	15.7169	15.4402	14.7298	14.8867	15.4669	15.479	14.0179	13.2984	15.6854	15.7161	14.9795	14.5015
MRPL3	12.2825	12.3729	11.0791	11.2918	11.9549	11.3625	10.914	10.9846	11.8626	11.8261	10.5385	10.1197	12.0486	11.9826	11.2309	10.794
RPL22	10.8556	10.9599	9.57923	9.82242	10.5016	10.1413	9.45934	9.76402	10.7432	10.8045	9.70276	9.19642	10.8207	10.7983	9.81038	9.45066
EEF2KMT	8.69	8.55165	7.64063	7.79689	8.59664	8.04155	7.56395	7.57389	7.9082	7.98651	6.65058	5.65288	8.0334	7.80545	6.76896	6.51488
RUVBL2	12.0133	11.8683	10.7809	10.8974	11.8813	11.6807	10.8442	10.9859	11.4088	11.2902	10.4717	10.1405	12.1284	12.1416	10.9334	10.7671
LIAS	8.93074	9.06483	8.23339	7.8392	8.65403	8.48185	7.86631	7.74625	9.46346	9.35151	7.79159	7.68651	9.58074	9.12852	8.48334	8.13718
XPOT	11.5684	11.466	10.5708	10.5339	11.4683	11.3746	10.4613	10.4852	12.5989	12.5084	11.2913	10.6706	12.6888	12.6996	12.093	11.626
NOB1	10.5068	10.5965	9.19995	9.40457	10.2201	9.70585	9.16379	9.32688	10.2162	10.2102	8.98533	8.78914	10.4637	10.3761	9.63896	9.35203
DFFA	12.1315	12.0398	10.9637	11.023	12.0511	11.6505	11.1681	11.1218	11.6586	11.6019	10.4131	10.0335	11.8207	11.7158	11.0403	10.6548
POLD2	11.5063	11.2919	10.1667	10.3324	11.1385	10.8453	10.2523	10.251	11.7507	11.6316	10.7539	10.2115	12.083	12.0392	11.1646	10.9164
YBX1	15.0723	15.1732	13.7994	14.1012	14.8902	14.5656	13.9136	14.0702	15.1286	15.0726	14.1658	13.7935	15.6702	15.6038	14.7027	14.4985
CCT7	13.7444	13.7329	12.6239	12.7405	13.4605	13.0605	12.4741	12.6586	13.6589	13.5602	12.4839	12.1649	13.9302	13.7668	12.9914	12.8378
SRM	13.3706	13.368	12.128	12.1024	12.6755	12.0038	11.8154	11.5518	13.4241	13.3577	12.3021	11.9525	13.5537	13.0781	12.6926	12.4011
PRMT5	9.94837	9.83526	8.67826	8.53386	9.57982	8.82762	8.38512	8.52169	10.1525	10.0326	8.98533	8.91931	10.41	10.1745	9.58827	9.35203
EIF3E	12.7087	12.7803	11.6132	11.9777	12.5809	12.3279	11.4936	11.7515	12.4454	12.3705	11.2711	10.9228	12.5251	12.4381	11.844	11.4309
CAD	12.0505	11.8764	11.127	11.1544	11.8571	11.6655	11.125	11.0293	12.3685	12.2615	11.0244	10.4198	12.5217	12.4568	11.8197	11.6
DHX33	11.3902	11.5225	10.268	10.6006	11.1906	10.5869	10.3224	10.3739	11.7884	11.9449	10.431	9.91931	11.7723	11.614	11.2511	10.8909
LRPPRC	11.8568	12.0174	10.9841	11.2994	11.7855	11.5934	11.0891	11.1849	12.8121	12.9836	11.4575	11.0677	12.9118	12.8986	12.2306	11.834
MDH2	12.9998	12.9576	11.989	12.0453	12.8224	12.7357	11.9659	12.1457	12.7221	12.5647	11.6389	11.2441	13.0264	13.0819	12.2486	12.1022
NPM1	15.6251	15.7651	14.3728	14.787	15.3295	15.0254	14.2499	14.5578	15.4326	15.4817	14.3599	14.0236	15.4873	15.2727	14.9281	14.7131
CCDC51	9.60548	9.49633	8.32747	8.6525	9.20785	8.85108	8.15141	8.41536	8.96684	9.16543	8.20517	7.92496	9.36973	9.32231	8.19098	8.48623
SERBP1	14.2652	14.3543	13.2217	13.5519	13.9674	13.8163	13.2284	13.3979	14.2313	14.3393	13.1534	12.7673	14.3932	14.3234	13.6885	13.3727
MCCC2	11.4929	11.6648	10.9742	11.2143	11.47	11.3665	10.7829	10.9554	11.2754	11.3412	9.92804	9.4872	11.4913	11.5491	10.6972	10.2523
MRPS25	10.3923	10.1792	9.17182	9.42138	10.1189	9.81575	9.24529	9.05513	10.4199	10.5206	9.52622	9.32797	10.7914	10.6936	10.0425	9.83194
CCDC124	11.8486	11.7516	10.6711	10.5757	11.247	10.8511	10.3058	10.4577	10.7755	10.6768	10.0343	9.81218	11.3464	11.2875	10.3539	10.4272
SSBP1	11.749	11.7966	10.5884	10.7709	11.2497	10.6962	10.3235	10.401	11.302	11.2531	10.6417	10.4128	11.7505	11.547	10.6148	10.5889
CCT4	12.7187	12.7575	11.8966	12.1295	12.4796	12.2004	11.6619	11.8234	12.7247	12.7181	11.4898	11.1953	12.6994	12.6358	11.9983	11.7305
PDHA1	11.445	11.4959	10.6732	10.8055	11.4046	11.1875	10.6045	10.7831	11.2414	11.2162	10.3047	9.89218	11.65	11.7097	10.8556	10.609
CCT2	12.9388	13.0483	11.9643	12.2512	12.6442	12.2348	11.9789	11.9115	13.0981	13.1814	12.0253	11.6668	13.0702	12.9622	12.5357	12.2169
CSE1L	12.42	12.6182	11.5561	12.0059	12.3566	12.279	11.7623	11.8125	12.5748	12.5426	11.3877	11.0523	12.6566	12.5365	12.0551	11.6924
MYC	13.4584	13.3451	12.7174	12.714	12.6924	12.5722	11.8446	12.3535	13.004	12.9069	11.8021	11.3554	13.1168	13.1021	12.3973	12.3597
ATIC	12.445	12.3055	11.3719	11.6376	12.1739	11.9392	11.3665	11.6194	12.1495	12.0337	11.0563	10.2559	12.0891	12.1105	11.5917	11.4022
MRPL16	10.4409	10.3858	9.34197	9.59687	10.1058	9.95488	9.44723	9.57389	10.4429	10.3851	9.75162	9.41681	10.6469	10.6046	9.74423	9.62973
LARP1	13.8332	13.8217	12.8904	13.0915	13.6622	13.3471	12.7576	12.9373	13.6894	13.695	12.7482	12.3892	13.8927	13.7999	13.475	13.2328
SLC25A5	13.0923	13.0578	12.2701	12.3434	12.9062	12.6797	12.1852	12.3299	13.0931	12.9491	12.2542	11.6469	13.4072	13.363	12.7991	12.5576
CDK4	11.294	11.2309	10.4762	10.4639	10.8958	10.4057	10.1301	10.0098	11.5488	11.4868	10.7182	10.3226	11.6459	11.6071	11.0425	11.0532
NAE1	11.3471	11.5256	10.6035	10.8914	11.291	11.1407	10.5451	10.6738	11.0739	11.1495	10.3068	9.98835	11.2681	11.2482	10.6907	10.525
DLD	11.6887	11.9503	11.2271	11.438	11.6164	11.6564	11.0761	11.1704	11.0181	11.0853	10.1538	10.1011	11.2851	11.3942	10.638	10.2547
RBM28	11.1674	11.2364	10.5669	10.6923	11.1655	11.0184	10.5834	10.6163	10.7901	10.6534	9.81477	9.40877	10.9295	10.9665	10.5833	10.1424
CHCHD3	11.8025	11.851	11.0116	11.1544	11.5681	11.3635	10.9545	11.0112	11.3756	11.3406	10.6981	10.3523	11.5898	11.5238	11.0359	10.8987
SRI	10.9388	11.0451	10.2411	10.5052	10.652	10.5542	9.81542	10.0233	10.0788	9.81775	9.41118	9.30866	10.343	10.2695	9.59816	9.46751
EIF3H	12.3373	12.4562	11.6436	11.9853	12.3286	12.3171	11.6225	11.9079	12.9316	12.9	12.2598	12.1607	13.2557	13.1618	12.6378	12.4631
CDC42SE	11.4574	11.4641	12.1814	12.0457	11.2235	11.2384	11.71	11.5979	11.7129	11.7673	12.1719	12.1234	11.4616	11.5461	12.3194	12.1952
VEZF1	9.88111	9.73398	10.6925	10.5183	9.50381	9.72978	10.4103	10.2338	9.55281	9.68551	10.078	10.0568	9.48623	9.42794	10.1034	10.2103

Supplementary Figure Legends:

Supplementary Figure S1. Genetic examination of MYC abnormality in ENKTL. FISH was performed by using MYC break-apart and fusion probes respectively in 60 cases. (A) representative figures for the fusion probe. (B) Left, a representative figure showing *MYC* gain (MYC-CN/Chr 8-CN <2); Right, a summary of the FISH results.

Supplementary Figure S2. Survival outcomes of patients receiving pegaspargase/asparaginase-based treatment. The patients were grouped by MYC expression status, and the PFS (A) and OS (B) curves are shown.

Supplementary Figure S3. MYC KD in NK malignancy cells with low and intermediate MYC Expression. YT, NK-YS, and SNK-6 cells were knocked down with MYC by siRNA mixture S1. (A) MYC protein levels were measured 24 hours after siRNA transfection. (B) Cell viability was measured 72 hours after transfection.

Supplementary Figure S4. Transcriptome alteration after MYC KD in NK malignancy cells. RNA-seq was performed to measure the transcriptome alteration after 24h of MYC KD in NK-92 and IMC-1 cells. (A) The volcano plots showing the relative gene expression of MYC KD to control cells. Those with expression levels ≥ 2-fold were subject to further analysis. (B) The significantly altered genes in NK-92 and IMC-1 were analyzed by GSEA, respectively, and the enrichment of the “MYC_targets” signature is shown. (C-D) The commonly down-regulated (C) and up-regulated (D) genes between NK-92 and IMC-1 cells were examined with molecular signature enrichment. The Venn diagrams show the relationship of the altered genes between these two cells, and the Hallmark gene sets were used for the signature analysis.

Supplementary Figure S5. Transcriptome alteration after 48h of MYC knockdown in NK-92 and IMC-1 cells. (A) The volcano plots showing the relative gene expression of MYC knockdown to control cells. Those with expression levels ≥ 2-fold were subject to further analysis. (B) The commonly down-regulated and up-regulated genes between NK-92 and IMC-1 cells were examined with molecular signature enrichment using the Hallmark gene set. (C) The Venn diagrams showing the common down-regulation and up-regulation between these two cells.

Supplementary Figure S6. CDK4 as a potential therapeutic target in ENTKL with MYC overexpression. (A) MYC-low NK malignancy cell lines YT and NK-YS as well as BL cell lines Namalwa and Raji were knocked down with MYC for 48h and examined with MYC, HK2, and CDK4 by WB. (B) NK malignancy cell lines were treated with increasing doses of benserazide for 72h and examined with cell viability by prestoblue assay. The cell lines are ranked by the area under curve (AUC) of the inhibition plot. (C) KHYG-1, NK-92, and IMC-1 cells were treated with palbociclib (1μM) and examined with MYC mRNA level by qRT-PCR after 24h and 48h of treatment, respectively. (D) Namalwa and Raji cells were treated with palbociclib and examined with MYC protein level by WB after 24h and 48h of treatment. (E) NK malignancy cells were subjected to double thymidine block and examined with MYC level by WB.

Supplementary Figure S7. Pathological examination for IMC-1 CDX model. (A-B) Spleen and liver involvement of the xenograft tumor cells. (C-F) IHC staining of CD3e, CD56, MYC, and Ki-67 in the liver with tumor involvement.

Supplementary Figure S8. Palbociclib treatment in the YT-CDX model. The volume of the subcutaneous tumor was calculated using the formula $V = (W^2 \times L)/2$, and compared between saline control and palbociclib-treated groups.

Supplementary Figure S1

A

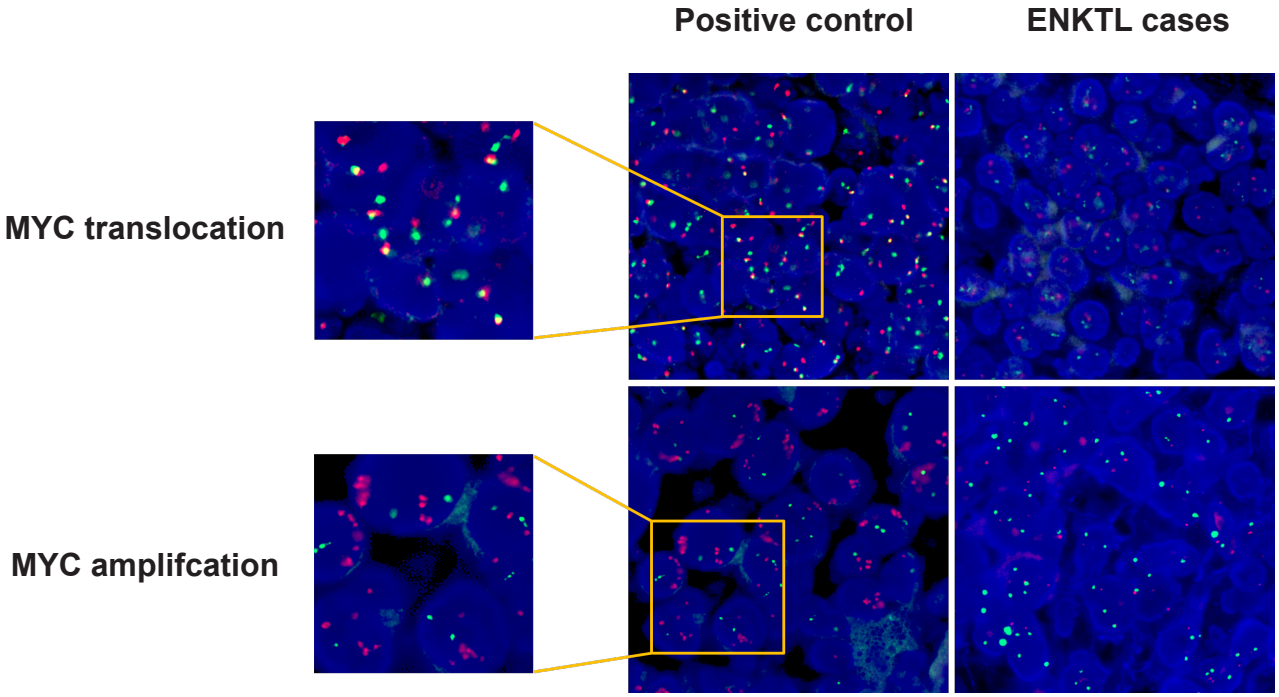

B

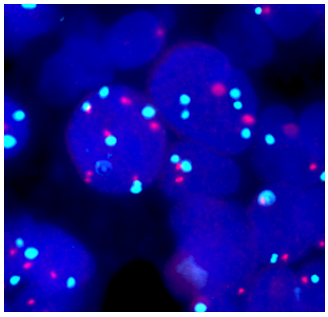

Genetic abnormality	Case number	MYC IHC
MYC translocation	0/60	N/A
MYC amplification	0/60	N/A
MYC gain	3/60	2/3

Supplementary Figure S2

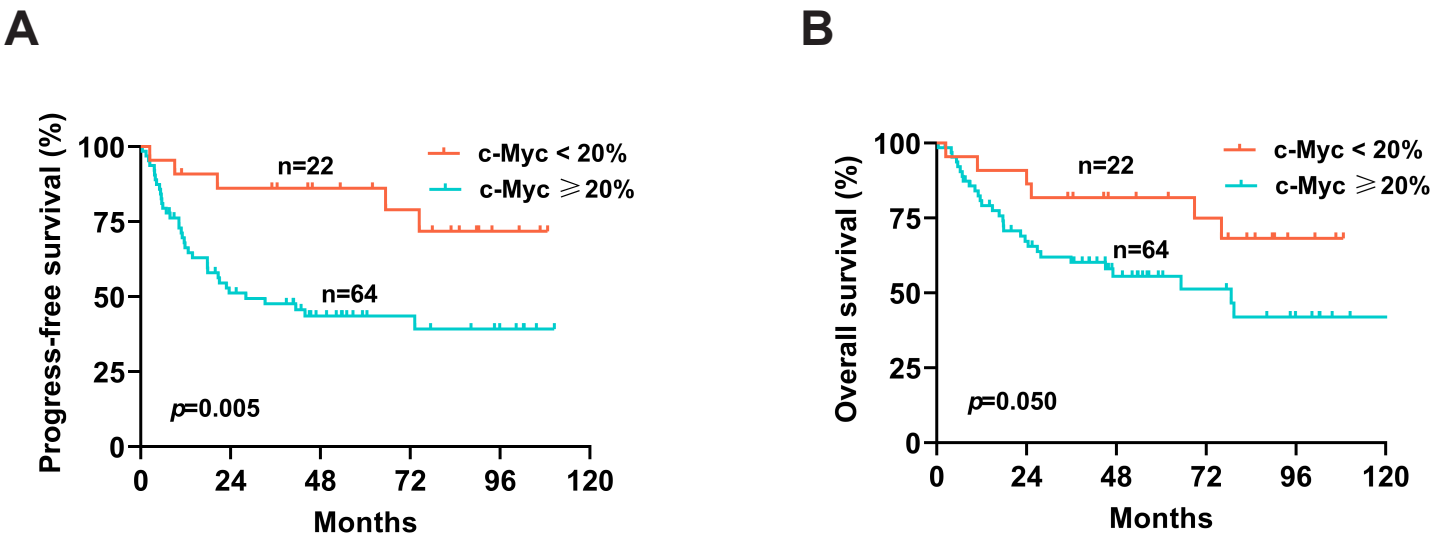

Supplementary Figure S3

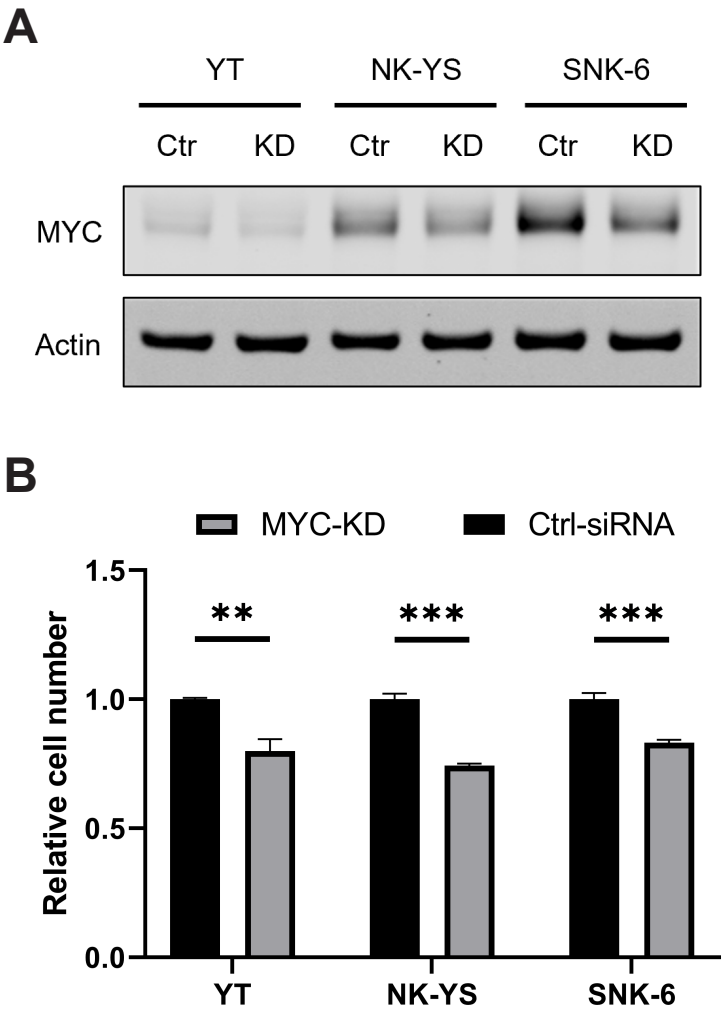

Supplementary Figure S4

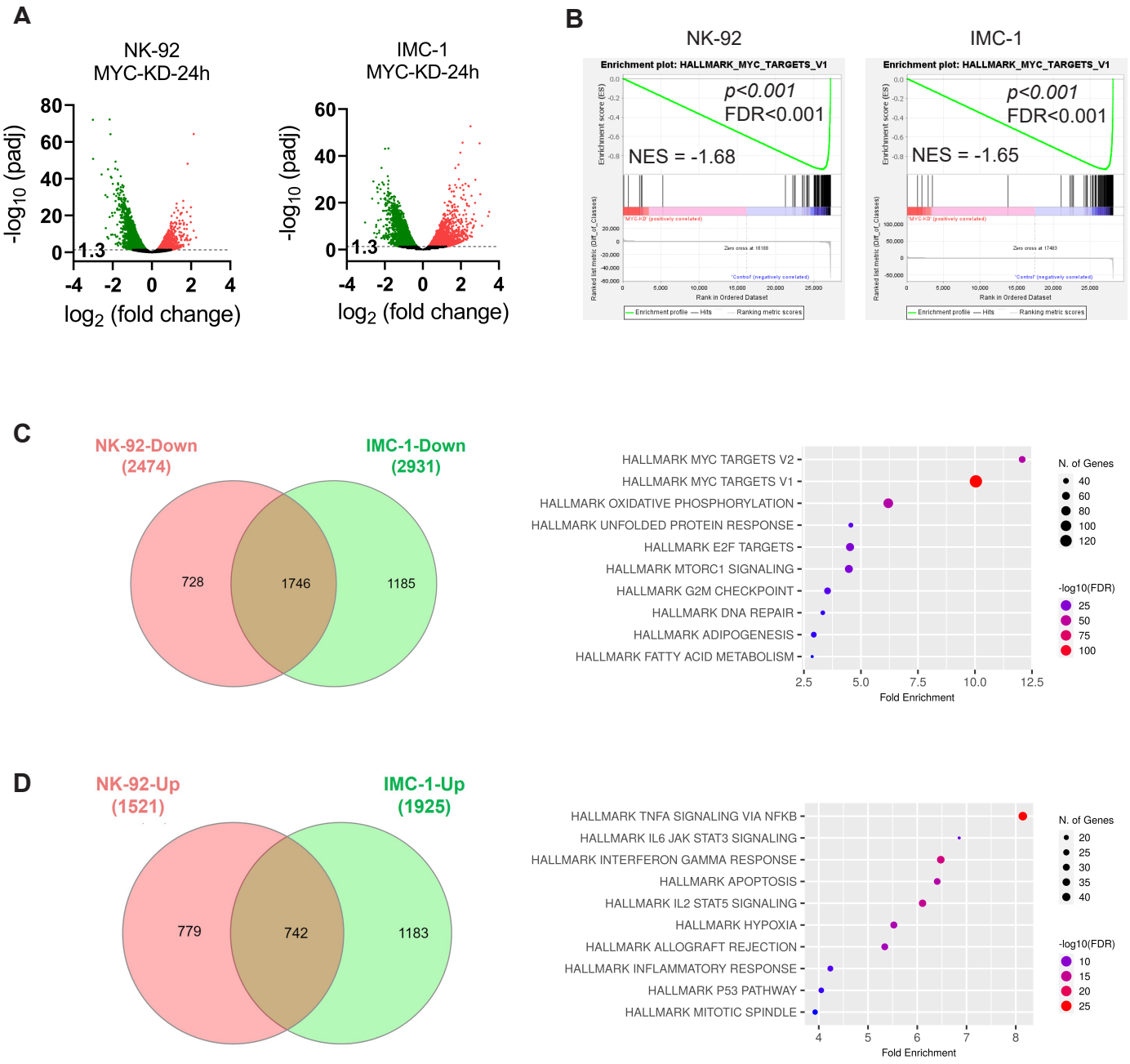

Supplementary Figure S5

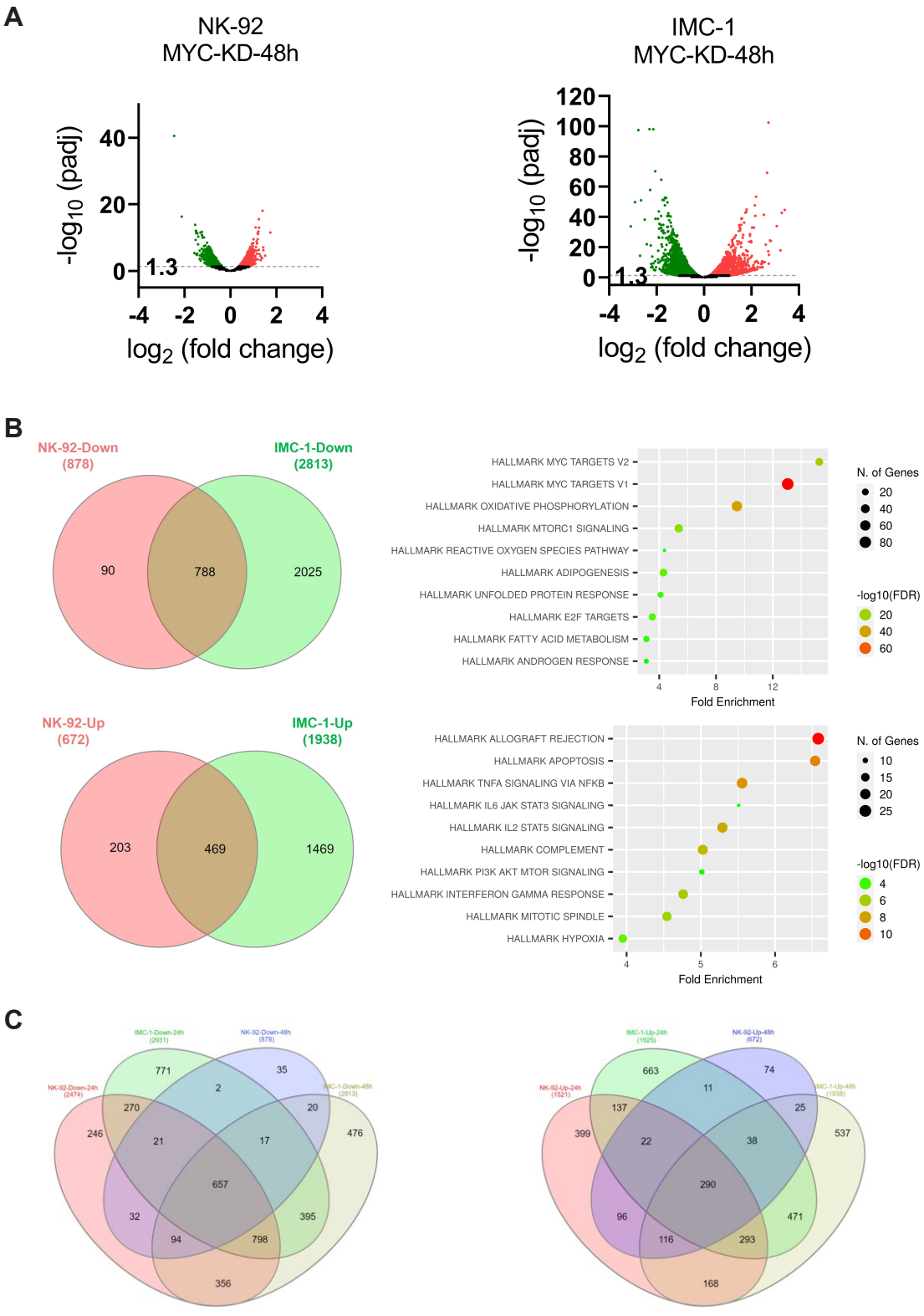

Supplementary Figure S6

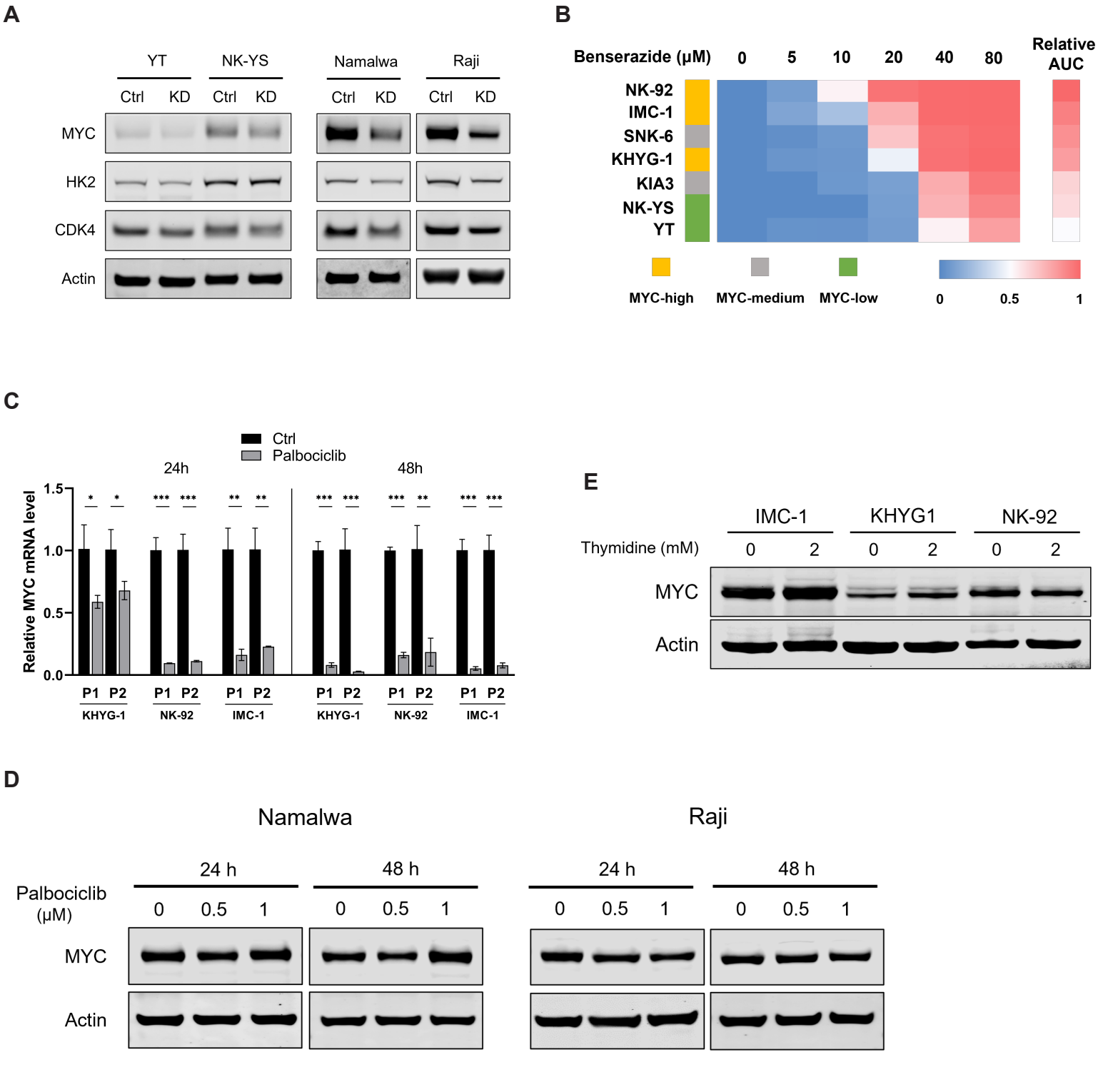

Supplementary Figure S7

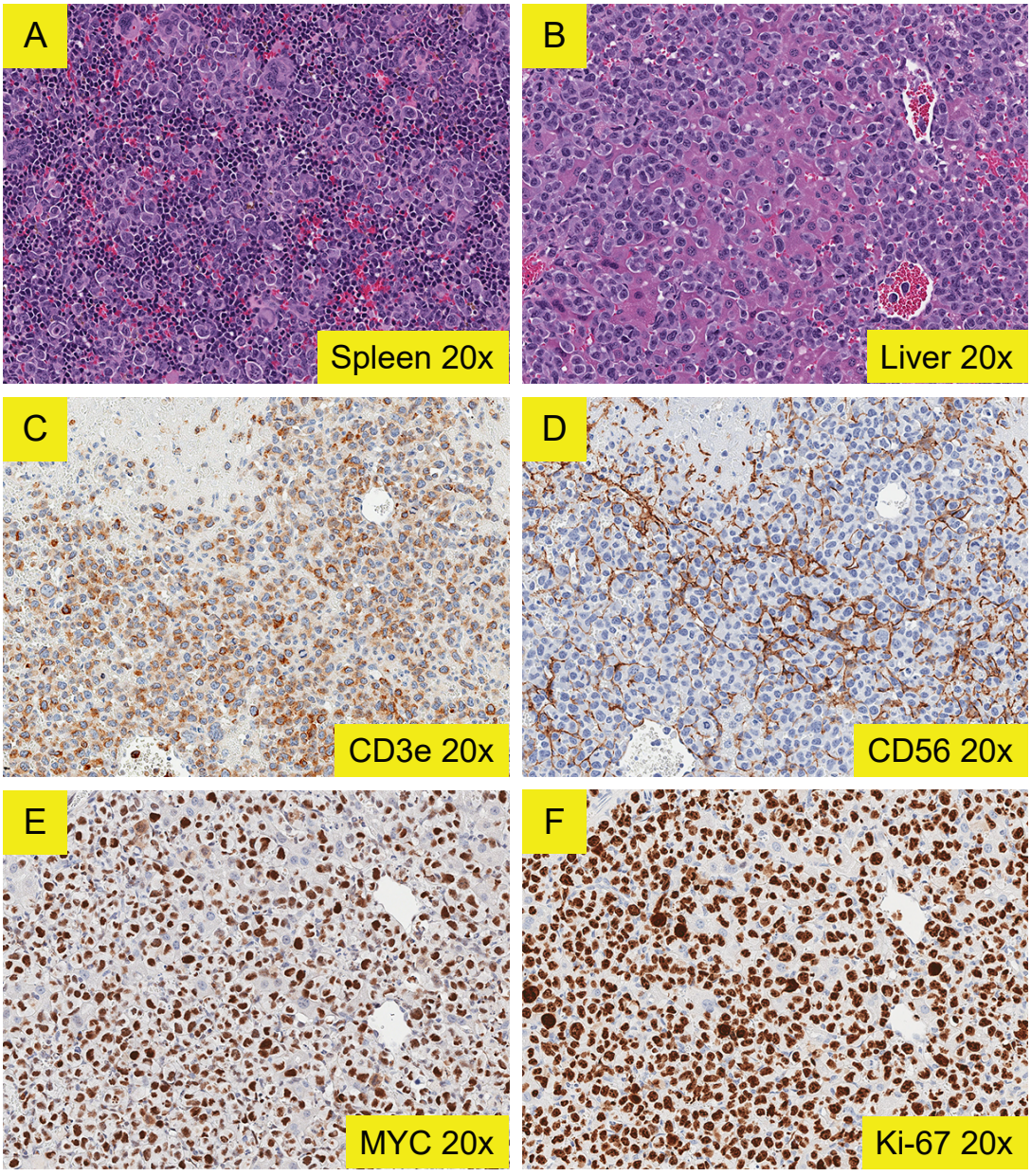

Supplementary Figure S8